

Development of a gene-editing approach to restore vision loss in Leber congenital amaurosis type 10

Morgan L. Maeder^{1,3*}, Michael Stefanidakis^{1,3}, Christopher J. Wilson¹, Reshica Baral¹, Luis Alberto Barrera¹, George S. Bounoutas¹, David Bumcrot¹, Hoson Chao¹, Dawn M. Ciulla¹, Jennifer A. DaSilva¹, Abhishek Dass¹, Vidya Dhanapal¹, Tim J. Fennell², Ari E. Friedland¹, Georgia Giannoukos¹, Sebastian W. Gloskowski¹, Alexandra Glucksmann¹, Gregory M. Gotta¹, Hariharan Jayaram¹, Scott J. Haskett¹, Bei Hopkins¹, Joy E. Horng¹, Shivangi Joshi¹, Eugenio Marco¹, Rina Mevani¹, Deepak Reyon¹, Terence Ta¹, Diana G. Tabbaa¹, Steven J. Samuelsson¹, Shen Shen¹, Maxwell N. Skor¹, Pam Stetkiewicz¹, Tongyao Wang¹, Clifford Yudkoff¹, Vic E. Myer¹, Charles F. Albright¹ and Haiyan Jiang¹

Leber congenital amaurosis type 10 is a severe retinal dystrophy caused by mutations in the CEP290 gene^{1,2}. We developed EDIT-101, a candidate genome-editing therapeutic, to remove the aberrant splice donor created by the IVS26 mutation in the CEP290 gene and restore normal CEP290 expression. Key to this therapeutic, we identified a pair of *Staphylococcus aureus* Cas9 guide RNAs that were highly active and specific to the human CEP290 target sequence. In vitro experiments in human cells and retinal explants demonstrated the molecular mechanism of action and nuclease specificity. Subretinal delivery of EDIT-101 in humanized CEP290 mice showed rapid and sustained CEP290 gene editing. A comparable surrogate non-human primate (NHP) vector also achieved productive editing of the NHP CEP290 gene at levels that met the target therapeutic threshold, and demonstrated the ability of CRISPR/Cas9 to edit somatic primate cells in vivo. These results support further development of EDIT-101 for LCA10 and additional CRISPR-based medicines for other inherited retinal disorders.

Leber congenital amaurosis type 10 (LCA10) is an autosomal recessive condition caused by bi-allelic loss-of-function mutations in the CEP290 gene. Most patients present clinically in early infancy with a severe cone-rod dystrophy and poor, to no, vision¹. The protein encoded by the CEP290 gene localizes to the photoreceptor-connecting cilium, and is required for outer segment regeneration and phototransduction^{1,2}. The most common LCA10-causing mutation is IVS26—an adenine to guanine point mutation located within intron 26 (referred to as c.2991+1655A>G) that creates a novel splice donor site, resulting in the inclusion of a 128 base pair (bp) cryptic exon (exon X) in the messenger RNA (mRNA) creating a premature stop codon^{3–9}. Aberrant splicing is more pronounced in human photoreceptors than in other cell types, explaining the retina-specific phenotype of the IVS26 mutation, relative to the syndromic disease more commonly associated with mutations resulting in complete inactivation of CEP290 (ref. ^{2,6,9–11}).

Currently, there is no approved treatment for LCA10. Although gene therapy is potentially curative, the large size of the CEP290 coding sequence (~7.5 kilobases) exceeds the packaging capacity of AAV. To overcome this limitation, we developed a gene-editing strategy specific for the CEP290 IVS26 mutation; EDIT-101 (Fig. 1a) uses an AAV5 vector to deliver the *Staphylococcus aureus* Cas9 and CEP290-specific guide RNAs (gRNAs) to photoreceptor cells by subretinal injection. We report the selection of two gRNAs, which are highly specific to the CEP290 locus, with no identified off-targets, and show that gene editing with these gRNAs corrects the CEP290 splicing defect. Since approximately 10% functional foveal cone photoreceptors is sufficient for near-normal visual acuity^{12,13}, we hypothesize that correction of the CEP290 IVS26 mutation in at least 10% of foveal cones will lead to clinical benefit in patients. Subretinal delivery of EDIT-101, or an NHP surrogate vector, was well tolerated and achieved sustained and dose-dependent CEP290 editing in photoreceptor cells, in mice and non-human primates, that met or exceeded the target therapeutic level.

On the basis of the molecular genetics and pathophysiology of LCA10-IVS26, we hypothesized that a pair of gRNAs to induce removal or inversion of the IVS26 mutation would result in normal splicing and subsequent restoration of functional CEP290 expression (Fig. 1b). The ability of both targeted deletions and inversions to functionally restore CEP290 splicing was demonstrated in a splicing reporter assay (Supplementary Results and Extended Data Fig. 1a,b). Transfection of SaCas9 and gRNA pairs into LCA10 patient fibroblasts resulted in increased expression of wild-type (WT) CEP290 mRNA and concomitant decrease in expression of the mutant transcript, as well as increased levels of full-length CEP290 protein (Fig. 1c, Supplementary Results, Supplementary Table 1 and Extended Data Fig. 2). On the basis of relative targeting efficiencies and a preliminary specificity assessment (Supplementary Table 2), CEP290 gRNAs 64 and 323 were selected as the lead candidate pair. These results demonstrate that targeted gene editing of the IVS26

¹Editas Medicine, Cambridge, MA, USA. ²Fulcrum Genomics, Somerville, MA, USA. ³These authors contributed equally: Morgan L. Maeder, Michael Stefanidakis. *e-mail: morganLmaeder@gmail.com

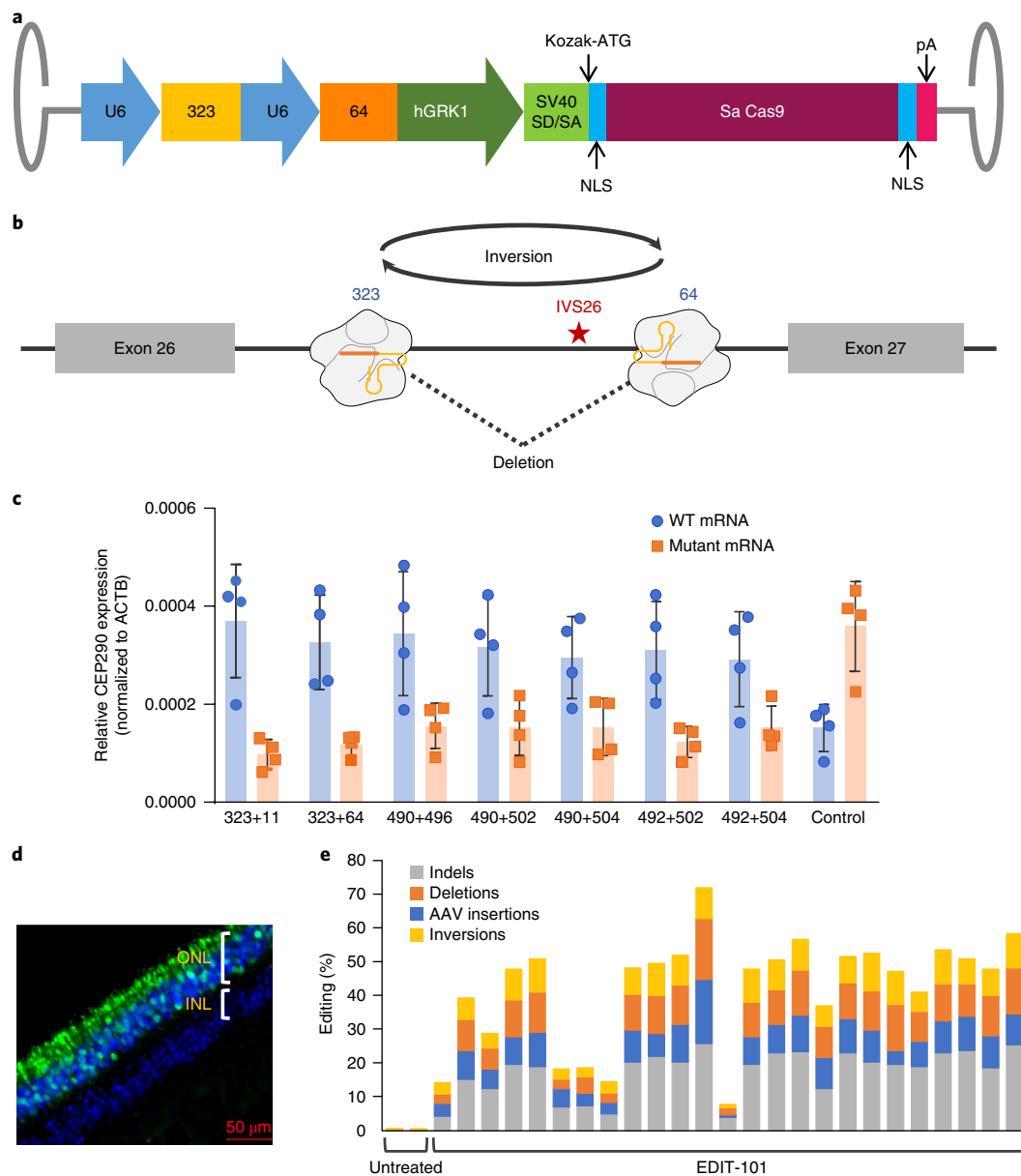


Fig. 1 | In vitro validation of EDIT-101. **a**, Schematic representation of EDIT-101, an AAV5 viral vector containing indicated components. U6: human U6 polymerase III promoter; 323: gRNA CEP290-323; 64: gRNA CEP290-64; hGRK1: human G protein-coupled receptor kinase 1 promoter; Kozak-ATG: consensus kozak sequence and ATG start codon; SV40 SD/SA: simian virus 40-splice donor and splice acceptor containing intronic sequence; NLS: nuclear localization signal; SaCas9: *Staphylococcus aureus* Cas9; pA: polyadenylation signal. **b**, Schematic of editing strategy. CEP290 gRNAs 323 and 64 flank the IVS26 mutation, while productive edits include deletion or inversion of the intervening sequence. **c**, Quantification of wild-type (WT, blue) and mutant (orange) CEP290 mRNA transcripts in IVS26#36 primary patient fibroblasts by quantitative PCR with reverse transcription (qRT-PCR). CEP290 expression is normalized to beta-actin (ACTB). $n = 4$ biological replicates (independent transfections performed on different days), qRT-PCR run in triplicate. Error bars represent standard deviation of the four biological replicates. The WT transcript is significantly increased and the mutant transcript is significantly decreased in all samples relative to control ($P = 0.008, 0.013, 0.021, 0.015, 0.007, 0.018$ and 0.011 for WT transcripts and $0.004, 0.007, 0.004, 0.009, 0.007, 0.005$ and 0.009 for mutant transcripts for pairs 323 + 11, 323 + 64, 490 + 496, 490 + 502, 490 + 504, 492 + 502 and 492 + 504, respectively, relative to control, two-tailed, paired t -test). **d**, Representative immunofluorescent imaging of human retinal explant histological section showing green fluorescent protein (GFP) expression in human explant treated with 1×10^{13} vg ml $^{-1}$ of AAV5-hGRK1-GFP. vg, viral genomes; ONL, outer nuclear layer; INL, inner nuclear layer. Green, GFP; blue, DAPI. The experiment was performed on three different explant punches. Scale bar, 50 μ m. **e**, Quantification of editing events in two untreated and 25 EDIT-101-treated human retinal explant punches from a single donor. Editing quantified by unidirectional targeted sequencing (UDiTaS)¹⁹.

mutation-containing region of CEP290 restores correct splicing and expression of CEP290, validating the molecular mechanism of our gene-editing strategy.

To demonstrate efficacy in mature human photoreceptors, a retinal explant culture system was developed. Transduction of retinal

explants with AAV5-GRK1-GFP showed that green fluorescence was observed exclusively in the photoreceptor-containing outer nuclear layer, confirming photoreceptor-specific activity of the GRK1 promoter (Fig. 1d). Retinal explants transduced with EDIT-101 revealed the expected spectrum of editing events, including

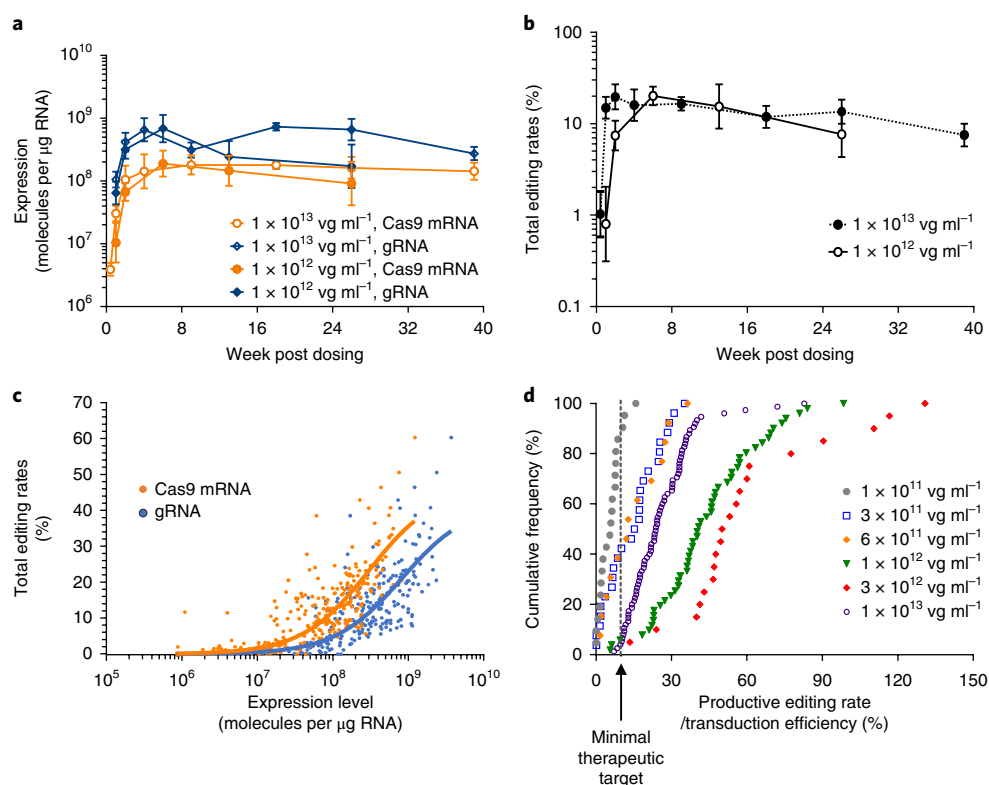


Fig. 2 | In vivo editing in HuCEP290 IVS26 knock-in mice. **a**, Time course for SaCas9 mRNA (orange circles) and gRNA (blue triangles) expression following subretinal dose of EDIT-101. Animals were dosed bilaterally with $1\mu\text{l}$ of $1 \times 10^{13} \text{vg ml}^{-1}$ (open circles/triangles) or $1 \times 10^{12} \text{vg ml}^{-1}$ (shaded circles/triangles) EDIT-101 and assayed at the specified time points. Expression quantified by qRT-PCR for Cas9 mRNA and gRNA. $n = 8\text{--}10$ eyes. Graph depicts geometric mean with 95% confidence interval. **b**, Time course for gene editing following subretinal dose of EDIT-101 (same samples as in **a**). Editing analyzed by UDiTaS in animals treated with $1 \times 10^{13} \text{vg ml}^{-1}$ (open circles) or $1 \times 10^{12} \text{vg ml}^{-1}$ (shaded circles) of EDIT-101. $n = 8\text{--}10$ eyes. Graph depicts geometric mean with 95% confidence interval. **c**, Correlation between total CEP290 gene-editing rates and Cas9 mRNA (orange) and gRNA (blue) expression. Each point represents an individual mouse eye following subretinal injection of $1\mu\text{l}$ of EDIT-101 at dose concentrations ranging from $1 \times 10^{11} \text{vg ml}^{-1}$ to $1 \times 10^{13} \text{vg ml}^{-1}$ and harvested at various timepoints from 3 days to 9 months post-dosing. Editing was quantified by UDiTaS. Cas9 mRNA and gRNA expression were quantified by qRT-PCR, and the curve was fitted by a nonlinear regression model. **d**, Dose response of EDIT-101 in achieving productive CEP290 editing. Data show cumulative frequency distribution of treated eyes in relation to exact productive editing rate within each dose group. Animals were assayed at 6 weeks post-dosing or later, with additional time points at 1, 2 and 4 weeks for the $1 \times 10^{13} \text{vg ml}^{-1}$ dose group. Except for the lack of statistical significance between the 3×10^{11} and $6 \times 10^{11} \text{vg ml}^{-1}$ dose groups, the semi-log dose increase from $1 \times 10^{11} \text{vg ml}^{-1}$ to $3 \times 10^{12} \text{vg ml}^{-1}$ resulted in a statistically significant increase in productive editing rate as assessed by pairwise comparisons between doses using Dwass-Steel-Critchlow-Fligner multiple comparison analysis, $P < 0.01$.

indels, deletions, inversions and insertions of AAV vector sequences into the cut site (Fig. 1e). Across 25 EDIT-101-treated retinal explant punches from a single donor, the average total rate of editing was $41.7 \pm 15.9\%$ and the average rate of productive editing (inversions+deletions) was $16.6 \pm 6.5\%$. These data demonstrate the functionality of EDIT-101 in fully mature human photoreceptors.

To comprehensively characterize the specificity of gRNAs 323 and 64, we used a stepwise approach consisting of a discovery phase and a verification phase. In the discovery phase, candidate off-target sites were identified and selected using three orthogonal methods: *in silico* prediction of closely matched sites in the reference human genome, GUIDE-Seq and Digenome-Seq (Supplementary Results and Supplementary Tables 3–7). In the verification phase, the pooled list of candidate off-target sites from the discovery phase was assayed by targeted next-generation sequencing in U2OS and ARPE-19 cells lines, as well as in human retinal explant tissue from two donors (Supplementary Results, Extended Data Fig. 3b,c and Supplementary Table 8). Across both cell lines and explants none of the candidate sites successfully sequenced was verified as an off-target site, and a large percentage of the sites (84–88%) was below the 0.1% lower limit of detection.

In summary, the SaCas9 64 and 323 guides are highly specific and no off-target sites were verified in either multiple human cell lines or human retinal tissue.

We used a human CEP290 IVS26 knock-in mouse model¹⁴ to assess the kinetics and dose response of targeted gene-editing efficiency *in vivo* following the subretinal delivery of EDIT-101. To determine the kinetics of CRISPR/Cas9 expression and on-target editing *in vivo*, HuCEP290 knock-in mice were treated with $1\mu\text{l}$ of $1 \times 10^{12} \text{vg ml}^{-1}$ or $1 \times 10^{13} \text{vg ml}^{-1}$ of EDIT-101 and analyzed over an extended duration, from 3 days to 9 months. At the dose of $1 \times 10^{13} \text{vg ml}^{-1}$, Cas9 mRNA was readily detectable at day 3 post-injection and expression of both Cas9 mRNA and gRNA increased significantly by week 2 and stabilized thereafter. In the $1 \times 10^{12} \text{vg ml}^{-1}$ dose group, SaCas9 and gRNA expression had peaked by week 6 (Fig. 2a). The CEP290 gene-editing rates in the two dose groups were significantly different at the early time points up to week 2 (two-tailed *t*-test, $P < 0.01$). By week 6, the editing rate in the $1 \times 10^{12} \text{ml}^{-1}$ dose group had plateaued at $21.4 \pm 4.9\%$, which is comparable to the rate of $21.2 \pm 9.6\%$ achieved in the $1 \times 10^{13} \text{vg ml}^{-1}$ dose group at week 2. The peak levels of editing seen in both groups were maintained through the 6- and 9-month durations of the study,

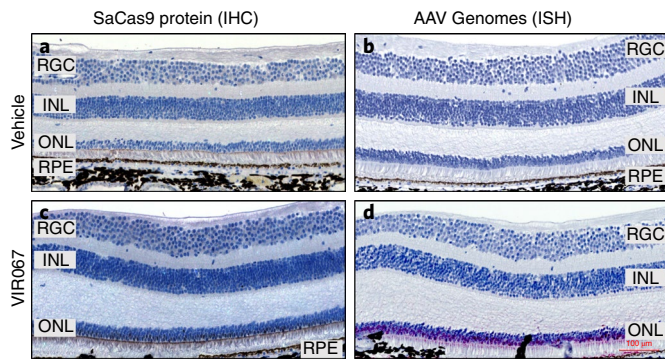


Fig. 3 | SaCas9 expression is restricted to photoreceptors in treated NHPs. a–d. Localization of SaCas9 detected by immunohistochemistry (a,c) and localization of AAV vector genomes detected by in situ hybridization (b,d) in NHPs treated with subretinal injection of balanced salt solution + pluronic vehicle (a, NHP no. 1008 OS; b, NHP no. 1007 OD) or subretinal injection of 7×10^{11} vg ml⁻¹ VIR067 (c,d, NHP no. 1012 OS). Zoomed from stitched $\times 20$ tiles. Scale bar, 100 μ m. ONL, outer nuclear layer; INL, inner nuclear layer; RGC, retinal ganglion cells; RPE, retinal pigment epithelium; IHC, immunohistochemistry; ISH, in situ hybridization. The experiment was performed on three treated retinas from three different animals (nos. 1010, 1011, 1012). OS: left eye; OD: right eye.

respectively (Fig. 2b). As shown in Fig. 2c, total CEP290 gene editing rates correlate with the levels of both SaCas9 mRNA and gRNA.

On the basis of published clinical observations, we hypothesized that the functional rescue of 10% of foveal cones would be necessary to achieve clinical benefit^{12,13}. To estimate the therapeutic dose range, we assessed the dose response of EDIT-101 ranging from 1×10^{11} to 1×10^{13} vg ml⁻¹ in achieving 10% or greater productive edits, which include the deletion and inversion of the CEP290 IVS26 target sequence normalized to the 30% transduction efficiency of the mouse retina (see transduction efficiency determination in Supplementary Results and Extended Data Fig. 4). The minimal therapeutic target was achieved in only a minority (14%, or 3/21) of eyes treated with 1×10^{11} vg ml⁻¹ of EDIT-101, whereas at 3×10^{11} and 6×10^{11} vg ml⁻¹, 62% of the treated eyes (16/26 and 8/15, respectively) achieved more than 10% productive editing. At doses of 1×10^{12} to 1×10^{13} vg ml⁻¹, 94% and above (48/51, 20/20 and 72/75) of the treated eyes achieved therapeutic target editing levels (Fig. 2d). The highest dose of 1×10^{13} vg ml⁻¹ resulted in a significantly lower productive editing rate compared with 1×10^{12} and 3×10^{12} vg ml⁻¹ dose groups, for reasons that are unclear at this time. These results predict that potential therapeutic efficacy may be achieved with EDIT-101 at a dose of 3×10^{11} vg ml⁻¹, and improved with increased doses up to 3×10^{12} vg ml⁻¹.

Mice lack a macula and >90% of their photoreceptor cells are rods, whereas the intended therapeutic target for LCA10 is foveal cones^{15,16}. It was therefore deemed critical to determine the level of productive editing in a retina anatomically similar to that of humans. Because of the sequence divergence between humans and NHPs, we developed a surrogate pair of gRNAs (cynoCEP290 gRNAs 21/51). AAV5 NHP vectors (VIR026 and VIR067) containing the same vector genome as EDIT-101, except for NHP CEP290 gRNAs 21/51 in place of HuCEP290 gRNAs, and the addition of a FLAG tag on the C-terminus of Cas9 in VIR026, were generated for subretinal injection in cynomolgus monkeys. These vectors had in vivo activity similar to that of EDIT-101 when tested in the humanized mouse model (Extended Data Fig. 5).

In two studies, NHPs were dosed subretinally and within the peri-foveal region with either 1×10^{11} or 1×10^{12} vg ml⁻¹ of VIR026 ($n = 3$ monkeys per group) or 7×10^{11} vg ml⁻¹ of VIR067 ($n = 3$ monkeys),

Table 1 | Editing rates in mice and NHPs at varying doses of EDIT-101 and surrogate vector

Vector dose (vg ml ⁻¹)	Productive editing rate in EDIT-101-treated mice (%)	Productive editing rate in surrogate-treated NHPs (%)
1.00×10^{11}	5.5 ± 4.1	3.5 ± 5.5
3.00×10^{11}	14.8 ± 10.6	
6.00×10^{11}	15.7 ± 11.5	
7.00×10^{11}		16.1 ± 2.8
1.00×10^{12}	44.2 ± 20.3	27.9 ± 20.7
3.00×10^{12}	60.8 ± 30.2	
1.00×10^{13}	25.8 ± 13.5	

Average in vivo editing rates (% \pm s.d.) in mice or NHPs subretinally injected with 1 μ l EDIT-101 or 100 μ l surrogate vector at indicated doses (vg ml⁻¹). Editing was quantified by UDiTaS, and productive editing was determined by adding the rates of targeted deletion and inversion and then multiplying by 3.3 to correct for 30% transduction of mouse retina or 30% of all cells being photoreceptor cells in NHP retinal punch. Data are averaged across all time points shown in Fig. 2d.

at an injection volume of 100 μ l per eye (Supplementary Table 9). Efficient delivery to photoreceptor cells in the retina was observed using in situ hybridization, which showed specific binding to the vector genomes predominantly in the outer nuclear layer, with some additional signal detected in retinal pigment epithelium (Fig. 3 and Extended Data Fig. 6). Staining for viral genomes extended from the injection site to the location of the optic nerve, and the area of vector genome-positive staining was comparable across dose groups (Supplementary Table 10). Cas9 protein was detectable in retinas from animals receiving both 7×10^{11} and 1×10^{12} vg ml⁻¹, specifically in the photoreceptor cells within the subretinal bleb (Fig. 3 and Extended Data Fig. 6). This restricted expression of SaCas9, within photoreceptors only, is consistent with previously published reports showing that subretinal injection of AAV5-GRK1-GFP in NHP results in GFP expression in photoreceptors only¹⁷.

On-target CEP290 gene editing, as determined by UDiTaS sequencing of the genomic DNA harvested from the neural retina punch within the bleb, was detected in all treated animals (Table 1). Since photoreceptors comprise approximately 30% of the neural retinal cells in the NHP macula punch from which genomic DNA was harvested, the productive CEP290 editing rate in photoreceptor cells was estimated with a multiplier of 3.3. Editing rates in primates show a dose response with productive editing rates of $3.5 \pm 5.5\%$, $16.1 \pm 2.8\%$ and $27.9 \pm 20.7\%$ (mean \pm s.d.) in the 1×10^{11} , 7×10^{11} and 1×10^{12} vg ml⁻¹ dose groups, respectively. Consistent with the findings in HuCEP290 IVS26 mice, the average productive editing rate in NHP at 7×10^{11} and 1×10^{12} vg ml⁻¹ would exceed the targeted minimum threshold of 10% anticipated as being clinically efficacious (Table 1).

Genome-editing technologies are now on the cusp of moving from a versatile research tool to realizing their full potential in the treatment of human genetic disease. As these programs advance towards patients, they are pioneering a new class of medicines and defining the scope of preclinical development of a gene-editing therapeutic. Here, we consider the unique challenges associated with CRISPR/Cas9 drug development and outline a generalizable framework for preclinical development of a gene-editing medicine.

One of the complexities of drug development for gene editing is that it is inherently human genome specific. We use human cells and tissue to demonstrate the therapeutic mechanism of action and to profile nuclease specificity. In vivo studies comprised a combination of EDIT-101 in humanized CEP290 mice, as well as a surrogate vector in non-human primates. Encouragingly, vector doses that achieve editing rates above the predicted therapeutic threshold

align between mice and NHPs, thus providing the basis for dose extrapolation to first-in-human trial. The data from both species demonstrate productive editing rates in >10% of photoreceptors, with doses ranging from 3×10^{11} to 3×10^{12} vg ml⁻¹, and this aligns well with the 5×10^{11} vg ml⁻¹ dose of voretigene neparvovec-rzyl (Luxturna, Spark Therapeutics)¹⁸.

EDIT-101 builds on the clinically demonstrated safety and efficacy of subretinally delivered AAV from other clinical programs. The localized delivery by subretinal injection, natural tropism of AAV5 for photoreceptor cells and the use of the photoreceptor-specific GRK1 promoter all serve to limit the expression of the CRISPR/Cas9 system to only the therapeutic target tissue and cell type. To support the clinical development of EDIT-101, we conducted comprehensive studies to assess the tolerability of subretinally delivered EDIT-101. We show that there is no detectable adaptive immune response to SaCas9 in primates treated with EDIT-101 or NHP surrogate, and that despite immune response to AAV5, which is significantly higher in the absence of immunosuppression treatment, gene-editing efficiency remains high (Supplementary Results and Extended Data Figs. 7 and 8). Importantly, subretinal delivery of EDIT-101 was well tolerated in all animals with only mild inflammation observed in non-immunosuppressed animals, possibly as a result of immune response to AAV5 (Supplementary Results and Extended Data Figs. 9 and 10).

In summary, we describe here the proof of concept, pharmacology and comprehensive specificity and tolerability of EDIT-101 and, in doing so, provide a roadmap for the preclinical development of a gene-editing therapeutic. Importantly, we not only show gene editing in primate photoreceptors, but more broadly demonstrate the ability to edit the genome in primate somatic cells. This is a critical advance towards unlocking the potential of gene editing for human therapeutics. Overall, our results support further development of EDIT-101 for the treatment of patients with CEP290-associated retinal disease, as well as the application of gene-editing approaches to treating a wide variety of inherited retinal diseases.

Online content

Any methods, additional references, Nature Research reporting summaries, source data, statements of data availability and associated accession codes are available at <https://doi.org/10.1038/s41591-018-0327-9>.

Received: 3 August 2018; Accepted: 7 December 2018;
Published online: 21 January 2019

References

- Chang, B. et al. In-frame deletion in a novel centrosomal/ciliary protein CEP290/NPHP6 perturbs its interaction with RPGR and results in early-onset retinal degeneration in the rd16 mouse. *Hum. Mol. Genet.* **15**, 1847–1857 (2006).
- Drivas, T. G. & Bennett, J. CEP290 and the primary cilium. *Adv. Exp. Med. Biol.* **801**, 519–525 (2014).
- Stone, E. M. Leber congenital amaurosis - a model for efficient genetic testing of heterogeneous disorders: LXIV Edward Jackson Memorial Lecture. *Am. J. Ophthalmol.* **144**, 791–811 (2007).
- Stone, E. M. et al. Clinically focused molecular investigation of 1000 consecutive families with inherited retinal disease. *Ophthalmology* **124**, 1314–1331 (2017).
- Drivas, T. G., Wojno, A. P., Tucker, B. A., Stone, E. M. & Bennett, J. Basal exon skipping and genetic pleiotropy: a predictive model of disease pathogenesis. *Sci. Transl. Med.* **7**, 291ra297 (2015).
- den Hollander, A. I. et al. Mutations in the CEP290 (NPHP6) gene are a frequent cause of Leber congenital amaurosis. *Am. J. Hum. Genet.* **79**, 556–561 (2006).
- Collin, R. W. et al. Antisense oligonucleotide (AON)-based therapy for Leber congenital amaurosis caused by a frequent mutation in CEP290. *Mol. Ther. Nucleic Acids* **1**, e14 (2012).
- Gerard, X. et al. AON-mediated exon skipping restores ciliation in fibroblasts harboring the common Leber congenital amaurosis CEP290 mutation. *Mol. Ther. Nucleic Acids* **1**, e29 (2012).

- Parfitt, D. A. et al. Identification and correction of mechanisms underlying inherited blindness in human iPSC-derived optic cups. *Cell Stem Cell* **18**, 769–781 (2016).
- Coppieters, F., Lefever, S., Leroy, B. P. & De Baere, E. CEP290, a gene with many faces: mutation overview and presentation of CEP290base. *Hum. Mutat.* **31**, 1097–1108 (2010).
- Boye, S. E. et al. Natural history of cone disease in the murine model of Leber congenital amaurosis due to CEP290 mutation: determining the timing and expectation of therapy. *PLoS ONE* **9**, e92928 (2014).
- Geller, A. M. & Sieving, P. A. Assessment of foveal cone photoreceptors in Stargardt's macular dystrophy using a small dot detection task. *Vision Res.* **33**, 1509–1524 (1993).
- Geller, A. M., Sieving, P. A. & Green, D. G. Effect on grating identification of sampling with degenerate arrays. *J. Opt. Soc. Am. A.* **9**, 472–477 (1992).
- Garanto, A. et al. Unexpected CEP290 mRNA splicing in a humanized knock-in mouse model for Leber congenital amaurosis. *PLoS ONE* **8**, e79369 (2013).
- Cideciyan, A. V. et al. Centrosomal-ciliary gene CEP290/NPHP6 mutations result in blindness with unexpected sparing of photoreceptors and visual brain: implications for therapy of Leber congenital amaurosis. *Hum. Mutat.* **28**, 1074–1083 (2007).
- Cideciyan, A. V. et al. Cone photoreceptors are the main targets for gene therapy of NPHP5 (IQCB1) or NPHP6 (CEP290) blindness: generation of an all-cone Nphp6 hypomorph mouse that mimics the human retinal ciliopathy. *Hum. Mol. Genet.* **20**, 1411–1423 (2011).
- Boye, S. E. et al. The human rhodopsin kinase promoter in an AAV5 vector confers rod- and cone-specific expression in the primate retina. *Hum. Gene Ther.* **23**, 1101–1115 (2012).
- LUXTURN (voretigene neparvovec-rzyl, package insert) (Spark Therapeutics, 2017).
- Giannoukos, G. et al. UDiTaS, a genome editing detection method for indels and genome rearrangements. *BMC Genomics* **19**, 212 (2018).

Acknowledgements

We thank B. Tucker and colleagues at the University of Iowa for the LCA10 patient fibroblasts, and the patients for their generous donation of biopsy samples. We thank B. Rabe for advice and technological assistance in establishing retinal explant model. We thank M. McCartney and N. Sprehe from Lions Eye Institute for Transplant and Research for invaluable help and services with human retinal explant experiments, and we thank the donors and their families for their generous donation. We thank our Editas colleagues P. Baciu, D. Balderson and G. Cox for helpful discussions and scientific input, and K. LeClair, W. Jaworowicz and G. Wilmes for helpful discussions and for manufacturing expertise and materials supply. This work was fully funded by Editas Medicine.

Author contributions

M.L.M., M.S., C.J.W., D.B., A.G., P.S., V.E.M., C.F.A. and H.J. conceived the strategy and designed experiments. M.L.M., R.B., A.D., A.E.F., S.W.G., J.E.H., S.J., R.M., D.R., S.S. and M.N.S. designed, performed and analyzed in vitro experiments. M.L.M., M.S., G.S.B., H.C., S.S., C.Y. and H.J. designed, performed and analyzed in vivo experiments. S.J.H., C.F.A. and H.J. designed, performed and analyzed immunogenicity experiments. M.L.M., C.J.W., L.A.B., D.M.C., J.A.D., V.D., T.J.F., G.G., G.M.G., H.J., E.M., T.T., D.G.T., T.W. and V.E.M. designed, performed and analyzed specificity studies. B.H. and S.J.S. performed and analyzed histology studies. M.L.M., M.S., C.J.W., C.F.A. and H.J. wrote, and all authors reviewed, the manuscript.

Competing interests

C.J.W., R.B., G.S.B., D.M.C., J.A.D., A.D., V.D., A.E.F., G.G., S.W.G., G.M.G., B.H., S.J., E.M., D.R., T.T., D.G.T., S.J.S., S.S., P.S., T.W., C.Y., V.E.M. and C.F.A. are current employees and shareholders of Editas Medicine. M.L.M., M.S., H.C., L.A.B., D.B., A.G., S.J.H., H.J., J.E.H., R.M., M.N.S. and H.J. are former employees and shareholders of Editas Medicine and were employed by Editas at the time this work was conducted. T.J.F. is a paid consultant of Editas Medicine. Editas Medicine has filed patents pertaining to the work described in this manuscript.

Additional information

Extended data is available for this paper at <https://doi.org/10.1038/s41591-018-0327-9>.

Supplementary information is available for this paper at <https://doi.org/10.1038/s41591-018-0327-9>.

Reprints and permissions information is available at www.nature.com/reprints.

Correspondence and requests for materials should be addressed to M.L.M.

Publisher's note: Springer Nature remains neutral with regard to jurisdictional claims in published maps and institutional affiliations.

© The Author(s), under exclusive licence to Springer Nature America, Inc. 2019

Methods

AAV vector preparation. Three plasmids containing AAV2 inverted terminal repeats (ITRs) and transgenes were constructed using the Gibson Assembly Method (PLA322: pAAV-U6-CEP290gRNAs323/64-GRK1-SaCas9; PLA339: pAAV-U6-cynoCEP290gRNAs21/51-GRK1-SaCas9-3xFLAG; PLA509: pAAV-GRK1-GFP). AAV5 was produced by either double- or triple-plasmid transfection of HEK293 or HEK293T cells with the transgene-containing plasmid and one or two helper plasmids containing AAV2 Rep, AAV5 cap and Ad5 helper virus genes. The vector was purified by iodixanol gradient ultracentrifugation followed by either concentration and buffer exchange using a Vivaspin 500, or by an additional ion exchange chromatography column and buffer exchange and concentration with tangential flow filtration. The final vector was formulated in balanced salt solution (Alcon) with 0.014% Tween20 or 0.001% poloxamer 188 and titered using qPCR. Purity was verified as >90% on an SDS-PAGE, 10% PAA gel with SYPRO Ruby staining, and endotoxin levels were determined to be <0.5 endotoxin units ml⁻¹ by either Pierce LAL Chromogenic Endotoxin Quantitation Kit (Thermo Fisher) or Endosafe cartridges (Charles River Laboratories).

Human explant culture and transduction. Human cadaver donor eyes were obtained within approximately 5 h post-mortem by Lions Eye Institute. The neural retina was isolated and a 3 mm biopsy punch was used to take punches from the entire neural retina of both eyes. Retinal punches were transferred, with outer retina (photoreceptor side) facing downwards, on top of a nucleopore membrane in a 12-well tissue culture plate with sufficient media (DMEM/F12 + 10% fetal bovine serum + 1% L-glutamine + 1% penicillin/streptomycin) to moisten the membrane. Vector (10 µl at 5 × 10¹³ vg ml⁻¹) was pipetted between the neural retina and the nucleopore membrane such that it formed a viral bleb under the retinal tissue. Tissues were incubated at 37°C, 5% CO₂ for 1 h, then 2 ml of media was carefully added per well underneath the nucleopore membrane and tissues were incubated for 28 days, and medium was changed every 3 days. Tissues were collected and processed for either histology or molecular analysis. For histology, tissue was fixed in 10% neutral buffered formalin. For molecular analysis, tissue was snap-frozen in liquid nitrogen and processed for qRT-PCR and sequencing as described.

Cell culture and transfection. IVS26 patient fibroblasts (referred to as IVS26 nos. 35 and 36) were obtained from the University of Iowa and are described in ref.²⁰. All patients provided written, informed consent for the study, which was approved by the Institutional Review Board of the University of Iowa (project approval no. 200202022), and adhered to the tenets set forth in the Declaration of Helsinki. IVS26 patient fibroblasts were maintained in Gibco DMEM/F12 + glutamax (ThermoFisher), supplemented with 1% penicillin/streptomycin, 1% non-essential amino acids and 15% fetal bovine serum (Hyclone). IVS26 fibroblasts were transfected with a plasmid encoding SaCas9 driven by a cytomegalovirus promoter and linear DNA encoding gRNAs driven by the U6 promoter using the Lonza nucleofection system. Briefly, 2 × 10⁵ cells were resuspended in 20 µl P2 nucleofection solution, followed by the addition of 2 µg Cas9-encoding plasmid and 500 ng gRNA-encoding DNA (or 250 ng of each gRNA when used as a pair). Cells and DNA were transferred to a Lonza nucleocuvette. Cells were pulsed in a Lonza 4D nucleofector using pulse code DS-150. Following 10 min incubation at room temperature, 100 µl media was added and the cell suspension was transferred to one well of a 12-well culture plate containing media that had been pre-equilibrated at 37°C. Cells were incubated for 6–7 days post-transfection.

U2OS cells (ATCC) were cultured in Gibco DMEM supplemented with 1% penicillin/streptomycin and 10% fetal bovine serum. Transfection was performed using the 4D Lonza nucleofection system with SE solution and pulse code DN-100. For split-GFP reporter experiments, 2 × 10⁵ cells were transfected with 1 µg reporter plasmid and plated in 24-well plates. For editing experiments with targeted next generation sequencing, 1 million cells were transfected with 2,500 ng of SaCas9 and 1,250 ng of gRNA expression plasmids and plated in six-well plates.

ARPE19 cells (ATCC) were cultured in DMEM/F-12, supplemented with 10% fetal bovine serum and 1% penicillin/streptomycin. Cells were transfected using the 4D Lonza nucleofection system. Briefly, 1 million ARPE-19 cells were transfected with 2,500 ng of gRNA expression plasmid and 3,750 ng of SaCas9 expression plasmid using the SF nucleofection solution and pulse code DN-100. Cells were plated in six-well plates.

SH-SY5Y cells (ATCC) were cultured in EMEM/F12 supplemented with 10% fetal bovine serum and 1% penicillin/streptomycin. Cells were transfected using the Lonza 4D nucleofection system. Briefly, 1 million cells were transfected with 2,500 ng of gRNA expression plasmid and 3,750 ng of SaCas9 expression plasmid using the SF nucleofection solution and pulse code CA-137. Cells were plated in six-well plates.

Double-mobilized whole blood (Hemacare, Inc.) was prepared for and subjected to CD34⁺ cell-positive selection using the reagents Miltenyi Prodigy and Miltenyi CliniMACS. CD4⁺ T cells were positively selected for from the negative fraction of the CD34⁺ cell isolation, again using Miltenyi Prodigy and Miltenyi CliniMACS. CD4⁺ T cells were concentrated to 5 × 10⁷ ml⁻¹ in human AB serum supplemented with 10% DMSO using a controlled-rate freezer and stored long-term at -196°C. On the day of thawing, one vial of T cells was removed from liquid nitrogen and thawed using the ThawSTAR automated cell-thawing system;

3.31 × 10⁷ CD4 T cells were recovered from the thaw and combined with an equal number of anti-CD3/anti-CD28 activation beads in X-Vivo15 media supplemented with human AB serum, glutamax, N-acetyl-cysteine, IL-2, IL7 and IL-15 (stimulation media). Cells were plated in a non-tissue culture-treated T-75 flask at a concentration of 1.3 × 10⁶ cells ml⁻¹ and incubated at 37°C for 48 h. After 48 h, beads were removed from cells by magnetic separation. Cells were then removed from the stimulation media by centrifugation and re-plated in a non-tissue culture-treated T-75 flask at a concentration of 1.3 × 10⁶ ml⁻¹ in X-Vivo15 media supplemented with human AB serum, glutamax, N-acetyl-cysteine, IL-2, IL7 and IL-15 (expansion media). Cells were allowed to expand overnight for 24 h before transfection (see details in section on GUIDE-Seq method).

Genomic DNA and RNA extraction from cells. Genomic DNA was isolated using the Agencourt DNAdvance kit (Beckman Coulter) according to the manufacturer's instructions and quantified using Qubit fluorometric quantitation (ThermoFisher). Total RNA was isolated using either the Agencourt RNAdvance 2 kit (Beckman Coulter) or the RNEasy RNA Isolation Kit (Qiagen); DNase was treated with the Turbo DNA-free kit (Thermo Fisher Scientific).

Droplet digital PCR. To quantify targeted deletion rates when using gRNA pairs, droplet digital PCR was performed using the QX200 Droplet Digital PCR System from BioRad, with absolute quantification experiment type, using EvaGreen supermix according to the manufacturer's instructions. Quantification of reference and targeted deletion sequences was determined based on the number of positive droplets in each reaction using BioRad ddPCR software, and percentage deletion was calculated by dividing the rate of deletion sequences by that of reference sequences.

Western blotting. Cells were lysed in radioimmunoprecipitation assay buffer containing EDTA protease inhibitor, phosphatase, benzamide and MgCl₂. Protein lysates were quantified, run on a 3–8% tris-acetate gel and transferred to a polyvinylidene difluoride membrane using the BioRad semi-dry transfer system. After blocking, the membrane was incubated overnight at 4°C with a 1:250 dilution of CEP290 primary antibody (Abcam, no. ab128231). The following day, the membrane was washed and incubated with horseradish peroxidase-conjugated anti-rabbit secondary antibody for 1 h at room temperature. The blot was developed using a West Super Dura ECL kit. Blots were imaged and quantified on a ChemiDoc Imaging System using ImageLab software (BioRad).

Care and use of animals. All mouse studies were approved and governed by the Ediths Medicine and CRADL Institutional Animal Care and Use Committees. Human CEP290 IVS26 knock-in mice from a mixed C57BL/6, DBA2 and 129 OLA genetic background (B6;129S2-Cep290^{tm2.1Bwj})¹⁴ were provided by Radboud University Medical Center and bred at Taconic Bioscience. Heterozygous and homozygous knock-in mice for the human CEP290 IVS26 mutation were used at 6–12 weeks of age, and sexes were evenly distributed between groups.

The NHP studies were performed at Covance laboratory for study no. Covance 8346970, and at MPI Research for study no. MPI-2682-003 using cynomolgus monkeys (*Macaca fascicularis*) of Chinese origin. All procedures were approved by the Covance and MPI Institutional Animal Care and Use Committees, and in compliance with all regulatory requirements.

Subretinal injection in mice. Pupils were first dilated with 1% cyclopentolate and 2.5% or 10% phenylephrine. The mouse was subsequently anesthetized using an intraperitoneal injection of a ketamine/xylazine cocktail ((100–150)/(5–10) mg kg⁻¹). One or two drops of 0.5% proparacaine were applied to each eye. An incision approximately 0.5 mm in length was made with a microscalpel 1 mm posterior to the nasal limbus. A blunt-ended needle on a 5 µl syringe was inserted through the scleral incision, posterior to the lens, toward the temporal retina until resistance was felt. One microliter of the vector or vehicle control (containing 200 µg ml⁻¹ of sodium fluorescein) was then injected slowly into the subretinal space. The eye was examined, and the success of subretinal injection was confirmed by first flattening the cornea with a glass coverslip then visualizing the fluorescein-containing bleb through the dilated pupil with a Leica M620 TTS ophthalmic surgical microscope fitted with a Leica MC170 HD digital color camera and full-HD LCD 24 inch monitor (Leica Microsystems, Inc.). Eyes with severe hemorrhage or leakage of vector solution from the subretinal space into the vitreous were excluded from further study. After the procedure, Tobrex (tobramycin ophthalmic ointment, 0.3%) (Alcon) was applied to each treated eye. Eyes with substantial complications from the injection procedure, such as unresolved retinal detachments, large hemorrhages or excessive damage to the retina, were excluded from the study and subsequent analysis.

Statistical analysis of in vivo mouse data. A normality check was performed on all datasets using the Shapiro–Wilk test. The normality testing results showed that the data were not normally distributed and, based on this finding, we were unable to use parametric statistical tests that require assumption of normality. Therefore, we chose to use geometric means for descriptive statistics and the Kruskal–Wallis test for statistical comparisons. The Kruskal–Wallis test does not require assumption

for normality, and performs the test based on ranks of data. A significant result in the Kruskal–Wallis test indicated that at least one group was different in ranking from other groups in the test. However, this test does not identify the source of the difference, nor how each group is different from other groups. To further examine the differences between each pair of doses or each pair of time points, we used Dwass–Steel–Critchlow–Fligner multiple comparison analysis established on pairwise two-sample Wilcoxon comparisons (SAS SAS/STAT 13.1 User's Guide, 2013). This method calculates a Wilcoxon rank sum test statistic on each pair of groups and computes family-wise error-protected *P* values to reduce false discovery rates. Finally, to explore correlations among gene expression and dose responses, we used the Spearman rank correlation test. Spearman's correlation coefficient is a statistical measure of the strength of a monotonic relationship between paired data. All analyses were performed in SAS 9.4 (SAS Institute, Inc.).

Subretinal injection in NHPs at Covance Laboratory. For NHP studies, animals were anesthetized and the eyes were cleaned with a solution of approximately 1% povidone iodine and rinsed with sterile saline. An solution of approximately 2.5% povidone iodine was used at the dose site before injection. Pupils were dilated with a topical mydriatic agent. A disposable dual-bore injection needle (23-g, Dutch Ophthalmic Research Center) was introduced directly through the sclera in the superior temporal quadrant of the globe approximately 3 mm posterior to the corneal limbus, and was moved through the vitreous under visual control using a surgical microscope while viewing through the dilated pupil with a modified fundus-viewing lens placed on the cornea. The 41-g cannula tip was advanced from the 23-g needle until gently touching the retinal surface. The dose (100 μ l per eye) was injected through the neural retina into the subretinal space, resulting in a subretinal bleb spanning the macular region. The 41-g cannula tip was retracted and the 23-g needle was withdrawn. A topical antibiotic and steroid ointment (neomycin polymyxin B sulfate–dexamethasone ophthalmic, Neo Poly Dex) was instilled in each eye following all other post-dose ocular procedures on that day.

All animals were treated with topical ocular (twice daily) and systemic anti-inflammatories beginning on the day before dosing and for 1 week post-dose. Animals received flunixin systemically three times daily, topical administration of atropine ophthalmic solution in both eyes three times daily, and Neo Poly Dex in both eyes twice daily. Test article-treated animals also received 0.25 mg kg⁻¹ dexamethasone intramuscularly 1 day before dosing and 2 mg of dexamethasone by subconjunctival injection after dosing.

Subretinal injection in NHPs at MPI Research. Before the surgical dosing procedure, the animals were anesthetized and placed in dorsal recumbency. Topical proparacaine was applied to the right eye. The conjunctival fornices of the right eye were flushed with a 1:50 dilution of betadine solution/saline and the eyelid margins were swabbed with undiluted 5% betadine solution. The right eye was draped and a wire eyelid speculum inserted. The temporal bulbar conjunctiva was swabbed with undiluted betadine solution. A caliper was used to mark spots 3.0 mm posterior to the limbus on the superotemporal and inferotemporal bulbar conjunctiva, over the pars plana. Bipolar cautery was applied to the spots for hemostasis. Conjunctival forceps were used to fix the globe position with the left hand while a 25-g, valved, scleral port was advanced through the sclera and into the vitreous humor at each spot. A flat vitrectomy lens was placed on the cornea for visualization of the posterior segment. A 25-g illumination probe and a 25-g subretinal injection cannula were inserted through the ports. The injection cannula was positioned on the retina near the vascular arcades and 10–40 μ l of appropriate vehicle was injected under the retina until the fovea detached. The cannula was immediately retracted. Vehicles 1 and 2, respectively, were used for the right and left eye in Group 1; balanced salt solution was used for both eyes in Groups 2–4. A 50 μ l aqueous paracentesis was performed using a 30-g needle to lower intraocular pressure and allow additional fluid to be delivered to the submacular space. The subretinal cannula was placed in the same retinotomy site, and the vehicle or test article dose (100 μ l) was slowly delivered into the subretinal space to expand the subretinal bleb. The vitrectomy lens and scleral ports were removed from the right eye and the lateral canthotomy was sutured closed. Subconjunctival injections of gentamicin and triamcinolone acetonide were administered to the right eye. The animal was repositioned and the procedure was repeated for the left eye.

Ophthalmoscopic examinations were conducted on all animals, under ketamine sedation, by a board-certified veterinary ophthalmologist. Scoring of anterior and posterior changes was based on modifications to the Standardization of Uveitis Nomenclature, Hackett–McDonald and Semi-quantitative Preclinical Ocular Toxicology Scoring systems. The ophthalmologist observed both eyes using a handheld slit-lamp biomicroscope with a beam setting of 0.1 mm width and 10 mm height. The eyes were evaluated for aqueous flare, aqueous cells and vitreous cells. The scoring system is depicted in Supplementary Table 12.

Genomic DNA and RNA extraction from tissue. Mouse neural retinas were dissected and flash-frozen immediately after enucleation, then placed on dry ice and stored at –80 °C for DNA and RNA isolation. For NHPs, 6–8 mm retinal tissue punches were harvested from the site of injection (subretinal bleb region) and snap-frozen for DNA and RNA isolation.

Frozen retinal samples were pulverized using a Geno/Grinder 2010 (SPEX SamplePrep, LLC) at 1,250 revolutions per minute for 30 s and homogenized using a Qiagen Tissue Lyser II (Qiagen). The homogenized tissue was suspended in 1 ml phosphate buffered saline (PBS) and split into two tubes for RNA and genomic DNA extraction. Genomic DNA was isolated using the DNEasy Blood and Tissue Kit (Qiagen) according to the manufacturer's instructions and quantified using Qubit fluorometric quantitation (Thermo Fisher). Total RNA was isolated using the mirVana miRNA Isolation Kit, with phenol (Thermo Fisher) following the total RNA extraction protocol, according to the manufacturer's instructions, and DNase was treated with a Turbo DNA-free DNA removal kit (Thermo Fisher).

qRT-PCR. Ribonucleic acid was reverse transcribed using the SuperScript III First-Strand Synthesis SuperMix for qRT-PCR Kit (Thermo) according to the manufacturer's instructions, except that for experiments quantifying Cas9 mRNA and gRNA, 1 μ l of a 52.5 μ M stock of a gene-specific primer for reverse transcribing gRNA was included. qPCR was performed in triplicate on a CFX384 Real Time PCR Detection System (BioRad) using Taqman Universal PCR Mastermix (Thermo Fisher). Housekeeping gene controls were quantified using Thermo Fisher TaqMan Gene Expression Assay no. Mf04392546_g1 for NHPs, Thermo Fisher Mouse GAPDH Endogenous Control (no. 4352932E) for mice or the custom human glyceraldehyde-3-phosphate dehydrogenase or beta-actin assays listed in Supplementary Table 10. SaCas9 and gRNA were quantified using the custom primer/probe sets listed in Supplementary Table 10. Standards for Cas9 mRNA and gRNA were plotted with a log₁₀ (ng) scale on the *x* axis and average cycle threshold (Ct) from the triplicates on the *y* axis with a linear trend line. The equation from the linear trend line of the standards was used to calculate the amounts (in nanograms) of Cas9 mRNA or gRNA present in experimental samples.

UDiTaS sequencing and data analysis. Editing at the human CEP290 locus was measured using the UDiTaS sequencing method as described in ref. ¹⁹. For NHP samples, *M. fascicularis* (genome build MacFas5) was used as reference, and primers OLI4604 and OLI4607 (Supplementary Table 10) were used in the UDiTaS reactions. Briefly, the analysis steps are as follows:

Demultiplex. Download raw fastq data. De-multiplex fastq files using the list of barcodes for each sample and extract the unique molecular identifiers (UMI) contained in the index files.

Trim. Remove 3' adapters using cutadapt.

Align to AAV plasmid. With bowtie2, index the AAV production plasmid sequence and then do a local alignment of the reads.

Filter and count reads aligning to AAV. Of the reads that locally align to the AAV plasmid, first filter out those where the 15 bases directly adjacent to the guide 323 anchor primer (on read 2) are not identical to the expected sequence. This removes reads that are due to false priming and ensures that at least 15 bp of sequence is present beyond the primer. Of the remain reads, collapse these by UMI and count the UMIs. Classify the exemplar read for each UMI as 'AAV/Plasmid Integrations'.

Extract unmapped reads. Extract the unmapped reads that did not locally align to the AAV/plasmid in steps 3 and 4 using bedtools bamtofastq.

Create reference amplicons. Build index files for the amplicons using bowtie2-index.

Align to reference amplicons. Align the unmapped reads from step 5 to the reference amplicons created in step 6 using bowtie2 in global mode (also known as end-to-end mode). Note that global mode requires both reads to be fully matching for the entire read. This is in contrast to local mode, where bowtie2 is allowed to trim the ends of reads.

Count reads in amplicons. Of the reads that align to the reference amplicons, collapse these by UMI and categorize an exemplar for each UMI to an aligned category—for example, Wild Type, Large Deletions and Inversion. Then count the number of UMIs per category.

Count small editing events. Extract the UMI-collapsed exemplar for reads aligned to the amplicons and identify reads where there is an indel \pm 15 bp at the expected cut site or junction.

The software used for the above analysis is available at <https://github.com/editasmedicine/uditass>.

Retinal dissociation and flow cytometry. Retinas were dissociated using the Papain Dissociation System (Worthington, no. 130-094-802) as described in Feodorova et al. with minor modifications²¹. Briefly, both retinas from each mouse were extracted by slashing the cornea with a scalpel and squeezing the retina through the opening with forceps. Retinas were kept in ice-cold PBS until ready for processing. Before processing, all dissociation reagents were equilibrated in a 37°C tissue culture incubator for 10–30 min. Retinas were then placed in 250 μ l Earle's Balanced Salt Solution (EBSS)/papain solution and incubated for 30 min at 37°C, with shaking at 350 revolutions per minute. Retinas were triturated with a 1 ml micropipette and transferred to a new tube containing a mix of EBSS, DNase and albumin-ovomucoid inhibitor. Retinas were triturated again with a 1 ml micropipette ten times. Finally, 250 μ l of EBSS/albumin-ovomucoid inhibitor was added and retinas were triturated with a 1 ml micropipette until tissue fragments were no longer visible. Dissociated cells were spun down at 350 g for 5 min,

resuspended in 0.5 ml Fixation Buffer (Biolegend, no. 420801) and incubated on ice for 20 min. Cells were spun down at 350g for 5 min and resuspended in 1.5 ml Cell Staining Buffer (Biolegend, no. 420201). The wash step was repeated two more times and cells were resuspended in a final volume of 0.5 ml Cell Staining Buffer. GFP-expressing cells were sorted using a Cell Sorter (Sony, no. SH800Z). Collected cells were spun at 350g for 5 min. The supernatant was discarded, and cells were snap-frozen and kept at -80°C until processed for DNA analysis. DNA was isolated from cells using the QIAamp DNA Micro Kit (Qiagen, no. 56304) according to the manufacturer's instructions.

Immunohistochemistry of Cas9 protein. Immunohistochemical staining was performed on paraffin sections of monkey neural retina (previously processed at Covance Laboratories). Briefly, eyes were fixed in 10% neutral buffered formalin for 24 h at 25°C , processed and then embedded in paraffin using a Tissue-Tek VIP processor. Sections ($5\ \mu\text{m}$) were mounted on glass slides, heated for 2 h at 37°C and shipped to Editas Medicine.

Sections were de-paraffinated and rehydrated by processing through xylenes and decreasing concentrations of ethanol in water. Endogenous peroxidase activity was blocked for 5 min with Peroxidase 1 (Biocare, no. PX968) followed by washing with distilled water. Tissue sections were then subjected to antigen retrieval using DIVA Decloaker (Biocare, no. DV2004) for 15 min at high temperature in a pressure cooker, followed by washing with distilled water and Tris buffered saline (Biocare, no. TWB945). Sections were then immunolabeled with rabbit monoclonal anti-Cas9 antibody (Abcam, no. ab203943) at $1\ \mu\text{g}\ \text{ml}^{-1}$ diluted in Renoir Red diluent (Biocare, no. PD904) for 2 h at room temperature. After washing in Tris buffered saline, antibody was detected with rabbit-on-rodent horseradish peroxidase-labeled polymer (Biocare, no. RMR622) for 30 min at room temperature, followed by Betazoid DAB Chromagen (Biocare, no. BDB2004) for 5 min. After rinsing with distilled water, slides were counterstained lightly with CAT Hematoxylin (CATHE, Biocare) for 5–7 s, blued using Tacha's Bluing solution (HTBLU, Biocare) for 10 s then dehydrated and coverslipped.

In situ hybridization of AAV vector genome. In situ hybridization was performed manually on paraffin sections of monkey neural retina (previously processed at Covance Laboratories) using the RNAscope 2.5 HD Red Reagent Kit (Advanced Cell Diagnostics, Inc.).

Slides of neural retina tissue sections and pellets of HeLa cells (for quality control; ACD, no. 310046) were baked for 1 h at 60°C and de-paraffinized with xylenes and ethanol. Endogenous peroxidase activity was blocked with RNAscope hydrogen peroxide (ACD, no. 322335) for 10 min at room temperature. Slides were then pretreated with RNAscope target retrieval solution (ACD, no. 322001) for 5 min at $99\text{--}100^{\circ}\text{C}$, followed by digestion with RNAscope Protease Plus (ACD, no. 322331) for 15 min at room temperature.

One of the two HeLa control sections was hybridized with either an ACD positive-control probe (probe symbol Mfa-PPIB, ACD, no. 424141) or ACD negative-control probe (probe symbol dapB, ACD, no. 310043). The retinal sections were hybridized with AAV vector genome-specific probe (probe symbol saCas9-O1-sense, ACD, no. 505631). All slides were incubated for 2 h at 40°C in a HyBEZ II oven (ACD) then sequentially amplified six times with the RNAscope 2.5 HD detection reagent kit (ACD, no. 322360) at 40°C , with appropriate washes between each step (RNAscope Wash Buffer, ACD, no. 310091). Hybridization signals were detected with a 1:60 mixture of Fast RED-B to Fast RED-A (RNAscope 2.5 HD detection reagent kit (ACD, no. 322360). Fast Red generates a distinct red precipitate visible under both bright-field and fluorescence microscopy. All sections were then counterstained with Harris hematoxylin (Thermo Scientific, no. 6765003) for 10 s, blued briefly in 0.002% ammonia water and dried completely at 60°C before coverslipping.

Immunofluorescent staining of human retinal punches. Mounting: punches were cryoprotected, first through 10% then 30% sucrose/phosphate buffer and frozen in Optimal Cutting Temperature mounting medium in dry ice-cooled isopentane. Punches were then cross-sectioned at 6–8 μm using a Leica cryomicrotome (Leica Microsystems) at -20°C . Sections were melted on to Super-Frost Plus slides (EMS) and stored at -80°C until needed.

Immunofluorescence: slides were quickly warmed to 37°C , then sections were encircled with a hydrophobic barrier and dried on a warmer at 37°C before rehydrating with PBS; staining was carried out in a moist, dark incubation chamber. Sections were permeabilized (0.1% Triton-X100) and nonspecific binding was blocked (2% bovine serum albumin/5% donkey serum/PBS) before labeling with anti-GFP (ab13970, AbCam). Following DAPI nuclear staining, sections were washed in PBS then TrisHCl and coverslipped under a hardening mounting medium (Prolong Diamond, ThermoFisher, no. P36961).

Imaging: multiplexed images were captured of GFP⁺ cells, antibody/probes and surrounding retinal layers as optical sections with a Zeiss Axio Imager M2 upright fluorescence microscope equipped with the Apotome2 optical sectioning device, and both a Zeiss 503 color camera and a Hamamatsu Flash 4.0 sCMOS monochrome camera. Multispectral images were captured using DAPI/ultraviolet (no. 365-395-445/50*) and GFP (no. 488 (470/40-495-525/50)), plus differential

interference contrast microscopy. Raw images were captured as .czi files then rendered for best fit with a micron bar and saved as .tiff files.

Ribonucleoprotein assembly. Ribonucleoprotein (RNP) was complexed from bacterially expressed and purified protein and chemically synthesized RNA oligonucleotides. In brief, RNA oligonucleotide was dissolved to 1 mM in H150 buffer (10 mM N-2-hydroxyethylpiperazine-N'-2-ethanesulfonic acid, 150 mM NaCl, pH 7.5), aliquoted and stored at -80°C until needed. When ready for use, RNA was thawed on ice and diluted to 0.75 mM in H150 buffer. RNA was then heated to 90°C for 5 min and slow-cooled to 25°C in a thermal cycler at a ramp rate of $4.68^{\circ}\text{C}\ \text{min}^{-1}$. SaCas9 protein (Aldevron) was subsequently concentrated to 0.4 mM and exchanged to HG300 buffer (50 mM N-2-hydroxyethylpiperazine-N'-2-ethanesulfonic acid, 300 mM NaCl, 1 mM tris(2-carboxyethyl)phosphine, 20% glycerol (9% v/v), pH 7.5), aliquoted and stored at -80°C . For RNP assembly, protein was thawed and then diluted to 0.375 mM. Equal volumes of protein at 0.375 mM and heated/slow-cooled RNA at 0.75 mM were mixed and incubated for 30 min at room temperature. RNP was then aliquoted and frozen at -80°C until ready for use.

Ribonucleoprotein was quality controlled using a differential scanning fluorimetry assay²³. In brief, complexed RNP was diluted to 2 μM in H150, and 5 μl of 2 μM RNP solution was subsequently added to 5 μl $\times 10$ Dye Mix in a 384-well plate. Alongside RNP, 5 μl of uncomplexed protein at 2 μM was added to 5 μl $\times 10$ Dye Mix as a control. The $\times 10$ Dye Mix was prepared by diluting $\times 5,000$ stock SYPRO Orange Protein Gel Stain (Life Technologies, no. S6651) in H150. The plate was sealed and briefly spun down, and the RNP-dye mix allowed to incubate at room temperature for 10 min, protected from light, to facilitate binding of the dye to RNP. The plate was then placed in a Bio-Rad thermocycler and the following protocol run: 1 min at 20°C , 20– 90°C at a ramp rate of $1^{\circ}\text{C}\ \text{min}^{-1}$ and 1 min at 4°C . Melt curves were generated from the negative first derivative of the raw fluorescence signal, and successful complexation was defined as a clear shift (increase) in melting temperature in the complexed RNP relative to the uncomplexed protein control.

Digenome-Seq. Digenome-Seq was adapted from ref. 23. RNP was prepared and stored as described in the previous section. Before initiating the cutting reaction, RNP was diluted to 2 μM in $\times 1$ H150 with 2 mM MgCl_2 and then serially diluted tenfold from 2.0 to 0.02 μM . Genomic DNA was purchased from Promega (no. G1521) and quantified in house using Invitrogen's Qubit Broad Range Kit (no. Q32850) following the manufacturer's protocol. Genomic DNA was diluted to 140 $\text{ng}\ \mu\text{l}^{-1}$ in Low TE buffer. Genomic DNA was then mixed volumetrically 1:1 with $\times 2$ H150 buffer with 4 mM MgCl_2 to prepare a 70 $\text{ng}\ \mu\text{l}^{-1}$ solution in $\times 1$ H150 with 2 mM MgCl_2 .

In one well of a 96-well plate, 5 μl of 70 $\text{ng}\ \mu\text{l}^{-1}$ genomic DNA prepared as described was mixed with 5 μl of RNP dilution or $\times 1$ H150 buffer with 2 mM MgCl_2 , creating a three-log dose response ranging from 1.0 to 0.01 μM for each RNP of interest and an untreated control. Twelve replicates were set up for each condition. The 96-well plate was incubated for 16 h at 37°C . Following incubation, the reaction was terminated by the addition of 2 μl of Proteinase K (800 units ml^{-1} ; NEB, no. P8107S) and subsequent incubation at 55°C for 30 min. To remove excess gRNA, 1 μl of RNase I(f) (50,000 units ml^{-1} ; NEB, no. M0234S) was added to each well followed by incubation at 37°C for 30 min.

Cut and control genomic DNA replicates were pooled, and the pool was purified using a $\times 1.8$ volume of Agencourt Ampure XP beads following the manufacturer's protocol. Purified genomic DNA was resuspended in Low TE and quantified using Invitrogen's Qubit Broad Range Kit following the manufacturer's protocol. One microgram of genomic DNA from each condition was submitted for PCR-free whole-genome 2×150 sequencing at Genewiz.

Sequencing data were aligned to GRCh38 using Burrows–Wheeler alignment mem version 0.7.17, and duplicate marked using Picard 2.17.0. Digenome-Seq analysis software is similar in concept to that presented in Park et al.²⁴, with the source code available from GitHub at <https://github.com/editasmedicine/digenomitas>. This analysis software scans the genome to identify loci with an enrichment of fragment ends starting at, and reading away from, the locus in the pattern expected for an unrepaired SaCas9 cut, and a depletion of fragments that are aligned spanning the locus, after filtering reads for low mapping quality and alignment artifacts caused by insertions and deletions proximal to the ends of sequencing reads. Putative cut sites are then filtered according to the number and fraction of fragments that appear to be cut at the site, the balance of coverage across positive and negative genomic strands, the overall depths of coverage and a computed score for the locus. Passing sites are given, along with the most likely alignment of the protospacer plus protospacer-adjacent motif to the cut site.

GUIDE-Seq. GUIDE-Seq was based on ref. 25 and performed as described in ref. 26 with the following differences. In cell lines and patient fibroblast lines, expression plasmids PLA348 (for guide 64) and PLA347 (for guide 323) were used; pAF003 was used for SaCas9 expression. In U-2 OS, ARPE-19 and SHSY5Y cells, donor double-stranded oligonucleotide was not the 5'3' double phosphorothioate, but 100 pmol of a 3' single phosphorothioate (OLI2924/OLI2925). In patient-derived fibroblast line no. 36, 25 pmol of the 3' double phosphorothioate (OLI2922/

OLI2923) was used. Nucleofection conditions were as follows: U-2 OS buffer SE program DN-100, ARPE-19 OS buffer SF program DN-100, SH-SY5Y buffer SF program DN-10 and patient-derived fibroblast line no. 36 buffer P2 program DS-150. For T cells, several conditions were run in parallel. In the nucleofection or electroporation well or cuvette, the 3' single phosphorothioate (OLI2924/OLI2925) was used at either 8 or 15 μM , and 5 or 10 μM RNP. Nucleofection with Lonza's Amaxa was carried out in the 96-well format and cuvette with the P2 buffer and DS130 pulse code, with 5×10^5 cells per well and 2×10^6 cells per cuvette, respectively. Electroporation in the Maxcyte system was done using the HT-1A pulse code and 4×10^6 cells per cuvette.

Sequencing libraries were created as previously described by Tsai et al.²⁵ with the following DNA shearing modification: 400 ng of genomic was sheared in 130 μl $\times 1$ TE Buffer (Tris-EDTA: 10 mM Tris base, 1 mM EDTA, pH 8.0) with adaptive focused acoustics (Covaris M220, Covaris, Inc.) (peak power, 50 W; cycles/burst, 200; duration, 60 s; duty factor, 10) to obtain 500 bp fragments. The sheared DNA was concentrated using AmPure XP beads (130 μl ; Beckman Coulter) following the manufacturer's specifications, and eluted in 15 μl $\times 1$ TE buffer. Adapter ligation, targeted amplification and sequencing were performed as previously described.

GUIDE-Seq analysis was performed as described in refs.^{25,26}. Briefly, reads were merged using PEAR (version 0.9.7, <https://sco.h-its.org/exelixis/web/software/pear/>), trimmed of adapters and double-stranded oligodeoxynucleotides using Cutadapt version 1.9.1 (ref.²⁷) and aligned to the hg38 reference genome using Bowtie2 version 2.1.0 (ref.²⁸). Finally, samtools (version 1.3-5-g664cc5f) was used to create and index-sort bam files²⁹. We selected regions passing the bidirectional filter²⁵, with at most six mismatches to the guide used in the experiment.

We calculated a relative lower limit of detection for each sample based on the number of unique on-target reads, assuming a binomial sampling distribution. The estimated lower relative limit of detection was calculated based on the cumulative probability mass function for a binomial distribution. Here, the probability of detecting at least two editing events occurring with frequency f given n samples (that is, unique reads) is given by $P = 1 - (1 - f)^n - nf(1 - f)^{n-1}$. To identify the lowest value of f detectable with 95% probability given n , the equation $0.95 = 1 - (1 - f)^n - nf(1 - f)^{n-1}$ can be numerically solved for f . Such a value for f is the lowest detectable frequency given the number of on-target unique reads for each GUIDE-Seq experiment.

Targeted sequencing of candidate off-target sites. For Illumina amplicon sequencing, two rounds of amplification were performed. Round 1 targets the off-target region while round 2 adds the full-length Illumina adapter sequence. Round 1 was performed in a 12 μl reaction volume, consisting of 6 μl Next Ultr II (NEB), Q5 Master Mix (New England Biolabs), 0.125 μM forward and reverse primer (see Supplementary Table 11 for primer sequences) and 20 ng gDNA template. PCR conditions were as follows: 30 s at 98°C for initial denaturation, followed by 20 cycles of 10 s at 98°C for denaturation, 15 s at 60°C for annealing, 30 s at 72°C for extension and 5 min at 72°C for the final extension. The PCR product was purified using $\times 0.9$ Agencourt AMPure XP beads (Beckman Coulter Agencourt, no. A63882) as per the manufacturer's protocol. Round 2 was performed in a 12 μl reaction volume, consisting of 6 μl Next Ultr II, Q5 Master Mix, 0.5 μM forward and reverse primers (see Supplementary Table 11 for primer sequences) and 20 ng gDNA template. PCR conditions were as follows: 30 s at 98°C for initial denaturation followed by 20 cycles of 10 s at 98°C for denaturation, 15 s at 60°C for annealing, 30 s at 72°C for extension and 5 min at 72°C for the final extension. The PCR product was purified using $\times 0.9$ Agencourt AMPure XP beads as per the manufacturer's protocol, followed by size selection (300–1200 bp) with BluePippin (Sage Science) and loaded on Illumina MiSeq with 10–20% phiX. Analysis of indel rates was performed as described in ref.³⁰, with the difference that reads were aligned to reference sequences using bowtie2, version 2.1.0 (ref.²⁸) rather than Needleman–Wunsch algorithm implementation in the EMBOSS suite v6.6.0.

A lower limit of detection was approximated at 0.1% editing, based on the following: (1) there were ~5,700 input haplotypes per PCR reaction, and (2) typical read counts were 10,000–100,000 per reaction and thus, assuming a binomial sampling distribution one would expect, with 95% confidence, at least 5 of 10,000 reads to contain indels for a 0.1% editing event (see also Supplemental Note in Kleinstiver et al.³¹).

In silico prediction of off-targets. Cas-OFFinder³² was used for off-target identification in the hg38 reference genome. To simulate DNA and RNA bulges, the protospacer sequence was modified by either removing single bases or adding gaps (represented by N in the sequence), respectively.

Anti-AAV5 antibody and anti-Cas9 antibody assays. AAV5- and Cas9-containing Luminex beads were generated according to the manufacturer's instructions. First, 12.5×10^6 beads were generated and stored at 4°C until use. AAV5 beads, designated 019, were labeled using 1×10^{13} vg ml⁻¹ AAV5. Cas9 beads, designated 015, were labeled using 2.5 μg ml⁻¹ Cas9 protein.

Study sera samples were diluted to between 1:20 and 1:6,250 in lysis buffer to obtain values within the linear range of the standard curve, and incubated with a 1:20 dilution of either AAV5- or Cas9-conjugated Luminex beads (12.5×10^6 ml⁻¹). To measure bound antibodies, 1 mM each biotinylated protein G

and streptavidin-PE were included in the assay. Plates were incubated overnight and analyzed the following day using the FLEXMAP 3D instrument. Samples were measured in technical and biological duplicates. The average and standard deviation of the resulting values are reported.

To construct a standard curve, anti-AAV5 (ADK5a) and anti-Cas9 (ED009) standards were diluted in lysis buffer in a 96-well plate at concentrations ranging from 0.338 to 20,000 ng ml⁻¹. These samples were then analyzed as above.

To determine anti-AAV5 and anti-Cas9 specificity, diluted samples were pre-incubated with either excess AAV5 (2×10^{13} vp ml⁻¹) or excess Cas ($160 \mu\text{g}$ ml⁻¹) for 1 h before incubation with the conjugated Luminex beads. These samples were then analyzed as above. Percentage inhibition was calculated using the formula $(1 - (\text{excess drug mean fluorescence intensity}/\text{no-drug mean fluorescence intensity})) \times 100$.

Enzyme-linked ImmunoSpot. Peripheral blood mononuclear cell samples, 500,000 cells per well, were incubated with Cas9 peptide pools (each peptide at a concentration of $10 \mu\text{g}$ ml⁻¹) in 96-well plates pre-coated with anti-IL2 and anti-IFN γ antibodies for 48 h at 37°C. Wells containing irrelevant antigens or media alone were used as negative controls. For positive controls, cells were incubated with cytomegalovirus peptides (PepMix), Concanavalin A and CEF peptides to elicit CD8 T cells, and CPI peptides for activation of CD4 T cells. Following incubation the cells were removed, the plates were washed and labeled cytokine-specific detection antibodies were added to the plates. Subsequently, plate-bound detection antibodies were visualized by enzymatic reactions. IL-2 (blue) and IFN γ (red) spots were detected and quantified using CTL ImmunoSpot alongside ImmunoSpot software.

For the peptide libraries, CD8⁺ peptide libraries containing 9-mer peptides overlapping by four amino acids were synthesized. The resulting 200 peptides were divided into six pools of 35 peptides each. CD4⁺ peptide libraries containing 15-mer peptides overlapping by ten amino acids were synthesized. The resulting 200 peptides were divided into six pools of 35 peptides each.

Reporting Summary. Further information on research design is available in the Nature Research Reporting Summary linked to this article.

Code availability

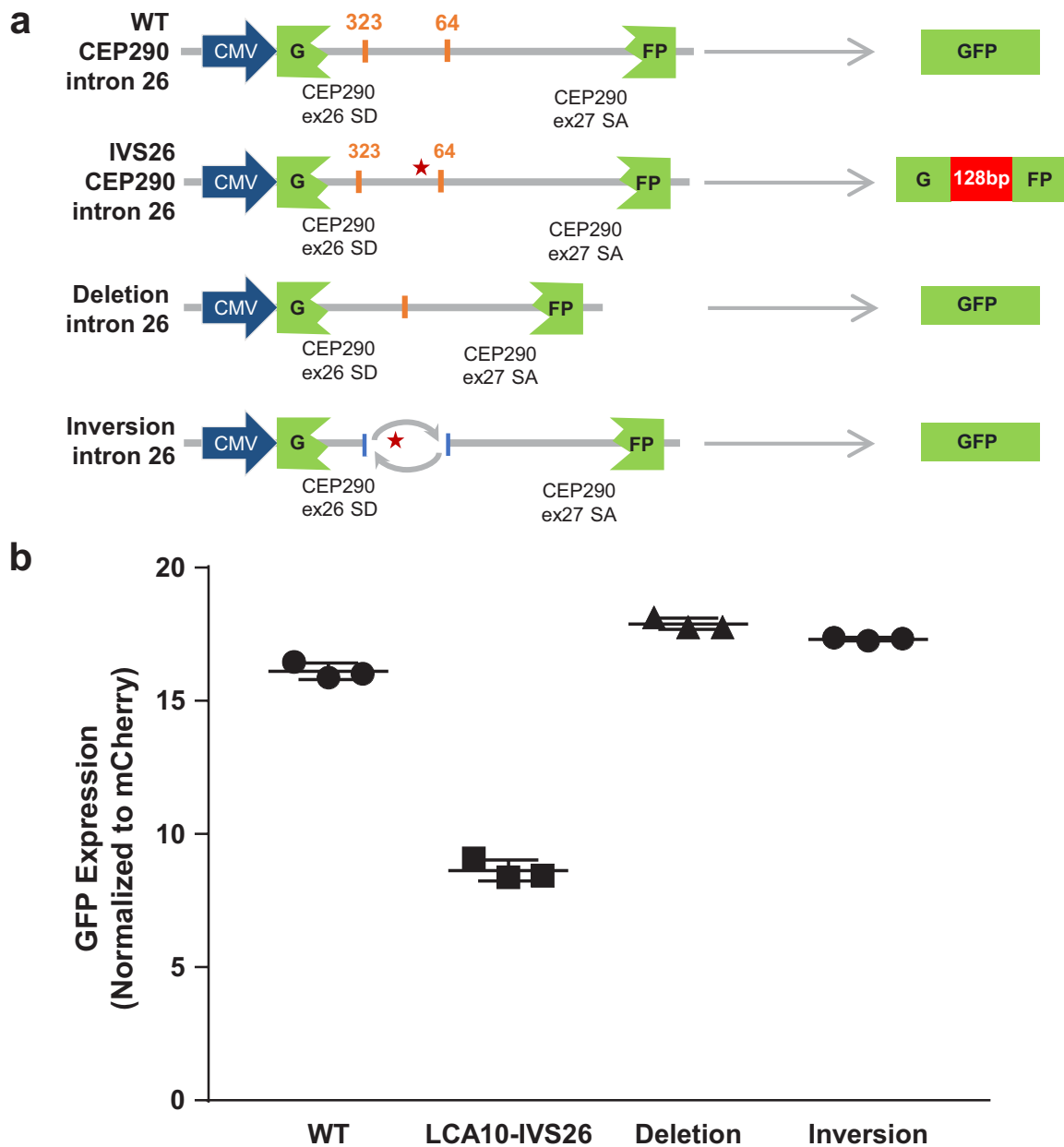
Custom analysis software is freely available at the following websites: <https://github.com/editasmedicine/uditas> <https://github.com/editasmedicine/digenomitas>

Data availability

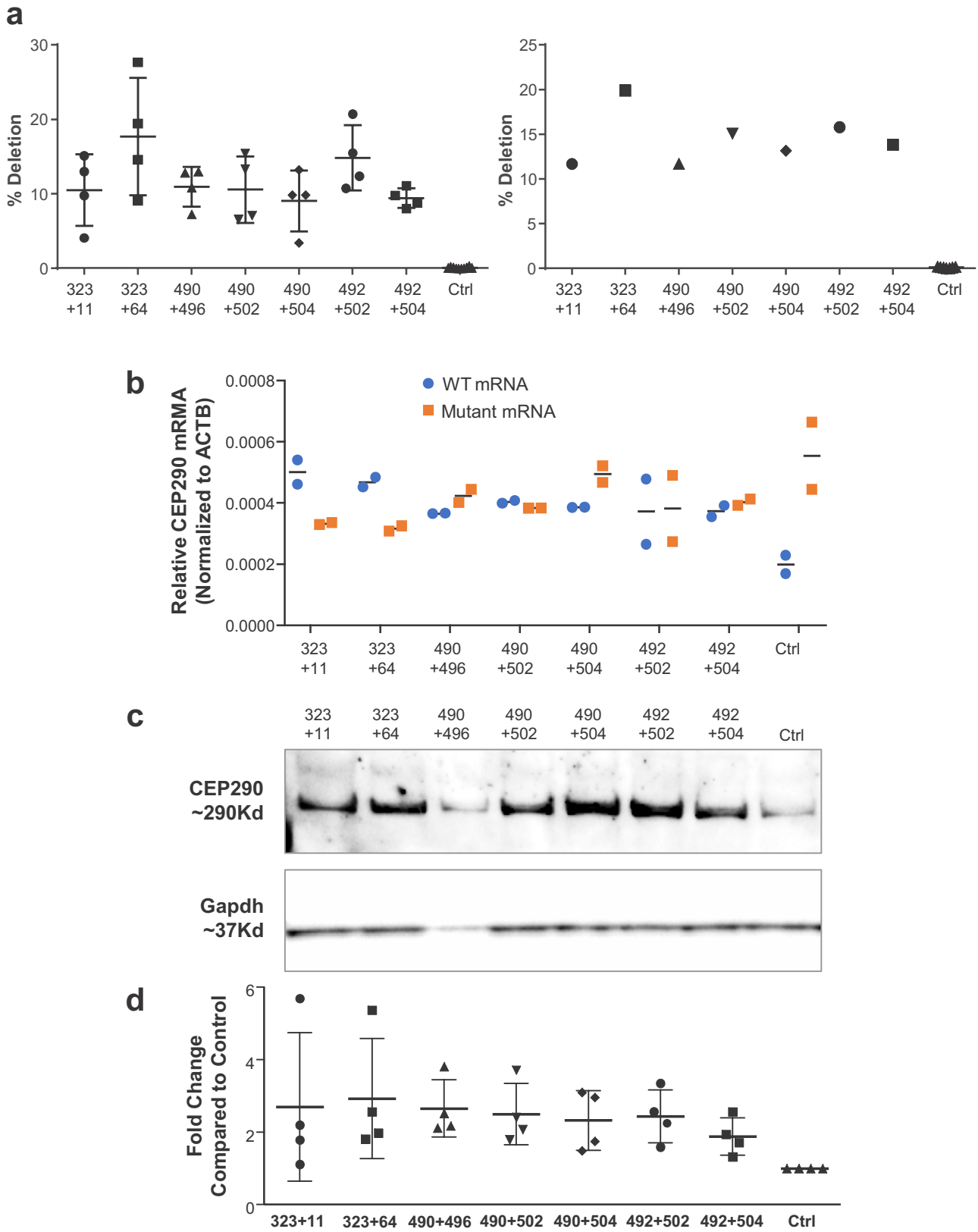
Detailed data analysis is available in the Supplementary Tables published with this manuscript. All requests for raw data are promptly reviewed by the CSO or CTO of Editas Medicine, and any data that can be shared will be released to the requestor. WGS data are available via the NCBI SRA database under accession code PRJNA497602.

References

- Burnight, E. R. et al. CEP290 gene transfer rescues Leber congenital amaurosis cellular phenotype. *Gene Ther.* **21**, 662–672 (2014).
- Feodorova, Y., Koch, M., Bultman, S., Michalakis, S. & Solovei, I. Quick and reliable method for retina dissociation and separation of rod photoreceptor perikarya from adult mice. *MethodsX* **2**, 39–46 (2015).
- Niesen, F. H., Berglund, H. & Vedadi, M. The use of differential scanning fluorimetry to detect ligand interactions that promote protein stability. *Nat. Protoc.* **2**, 2212–2221 (2007).
- Kim, D. et al. Digenome-seq: genome-wide profiling of CRISPR-Cas9 off-target effects in human cells. *Nat. Methods* **12**, 237–243 (2015).
- Park, J. et al. Digenome-seq web tool for profiling CRISPR specificity. *Nat. Methods* **14**, 548–549 (2017).
- Tsai, S. Q. et al. GUIDE-seq enables genome-wide profiling of off-target cleavage by CRISPR-Cas nucleases. *Nat. Biotechnol.* **33**, 187–197 (2015).
- Friedland, A. E. et al. Characterization of *Staphylococcus aureus* Cas9: a smaller Cas9 for all-in-one adeno-associated virus delivery and paired nickase applications. *Genome Biol.* **16**, 257 (2015).
- Martin, M. Cutadapt removes adapter sequences from high-throughput sequencing reads. *EMBO J.* **17**, 10–12 (2011).
- Langmead, B. & Salzberg, S. L. Fast gapped-read alignment with Bowtie 2. *Nat. Methods* **9**, 357–359 (2012).
- Li, H. et al. The sequence alignment/Map format and SAMtools. *Bioinformatics* **25**, 2078–2079 (2009).
- Bothmer, A. et al. Characterization of the interplay between DNA repair and CRISPR/Cas9-induced DNA lesions at an endogenous locus. *Nat. Commun.* **8**, 13905 (2017).
- Kleinstiver, B. P. Engineered CRISPR-Cas9 nucleases with altered PAM specificities. *Nature* **523**, 481–485 (2015).
- Bae, S., Park, J. & Kim, J. S. Cas-OFFinder: a fast and versatile algorithm that searches for potential off-target sites of Cas9 RNA-guided endonucleases. *Bioinformatics* **30**, 1473–1475 (2014).

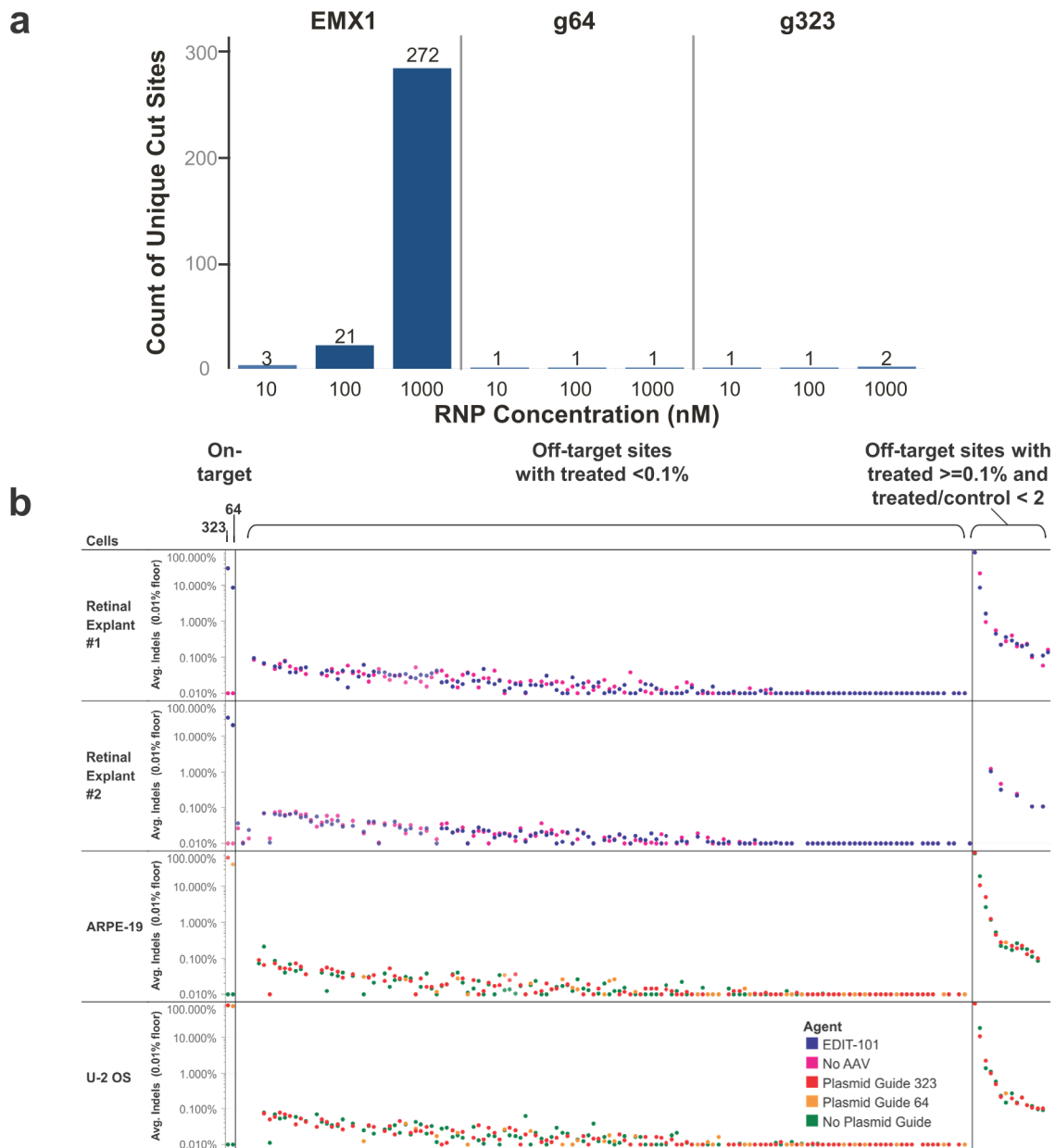


Extended Data Fig. 1 | Splicing reporter assay demonstrates functionality of deletions and inversions. **a**, Schematic depicting design of GFP reporter constructs to determine functionality of edits and ability to correct splicing. Cytomegalovirus promoter drives split GFP interrupted by a portion of CEP290 intron 26. Correct splicing is required to reconstitute GFP. **b**, Quantification of GFP expression (mean fluorescence intensity), normalized to PGK-mCherry also present on reporter plasmid, by flow cytometry following transfection into human U2OS cells. $n = 3$ independent transfections performed on separate days. Bars represent mean and standard deviation.



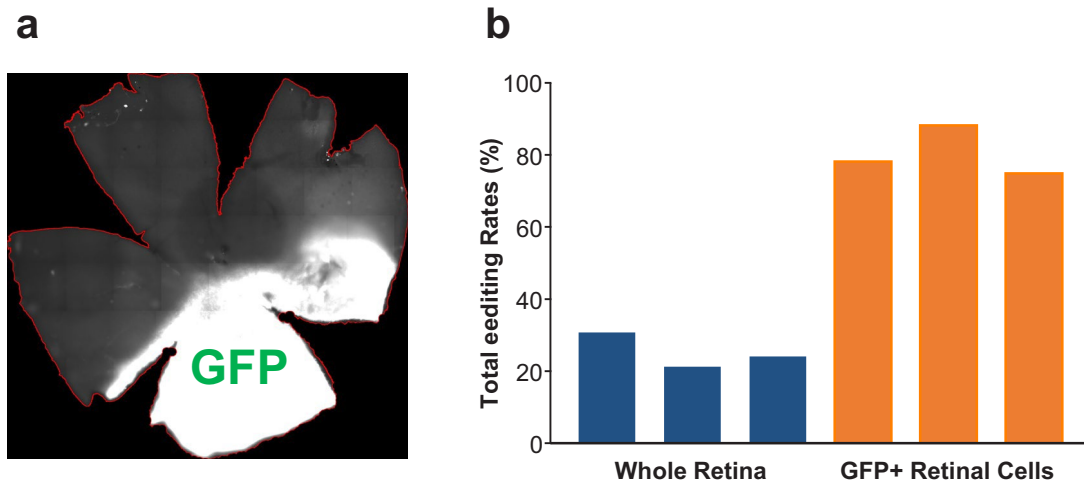
Extended Data Fig. 2 | see figure caption on next page.

Extended Data Fig. 2 | In vitro validation of editing strategy in primary patient fibroblasts. **a**, Targeted deletion at the CEP290 locus in primary patient fibroblasts transfected with plasmids encoding SaCas9 and seven different pairs of CEP290 gRNAs, as quantified by Droplet Digital PCR. Left, cell line IVS26#36, $n=4$ independent transfections performed on different days, error bars represent standard deviation. Right, cell line IVS26#35, $n=1$. **b**, Quantification of WT 26-27 (blue) and mutant 26-X-27 (orange) CEP290 mRNA transcripts in IVS26#35 primary patient fibroblasts by qRT-PCR. CEP290 expression is normalized to beta-actin. $n=2$ independent transfections performed on different days, qRT-PCR run in triplicate. Line represents mean. **c**, representative western blot from IVS26 primary patient fibroblasts transfected with plasmids encoding SaCas9 and seven different pairs of CEP290 gRNAs. Experiment was performed twice in each cell line with similar results. **d**, Quantification of CEP290 full-length protein expression in IVS26#36 and -#35 cell lines transfected with plasmids encoding SaCas9 and seven different pairs of CEP290 gRNAs. Expression level fold change over control calculated by densitometry of western blot bands and normalized to control. $n=4$ biological replicates (two different transfections on different days, each in the two different cell lines), error bars represent mean and standard deviation.

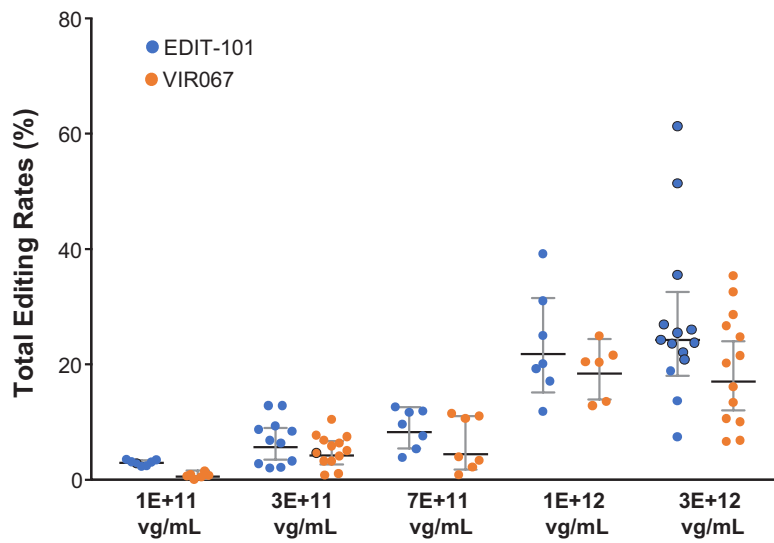


Extended Data Fig. 3 | see figure caption on next page.

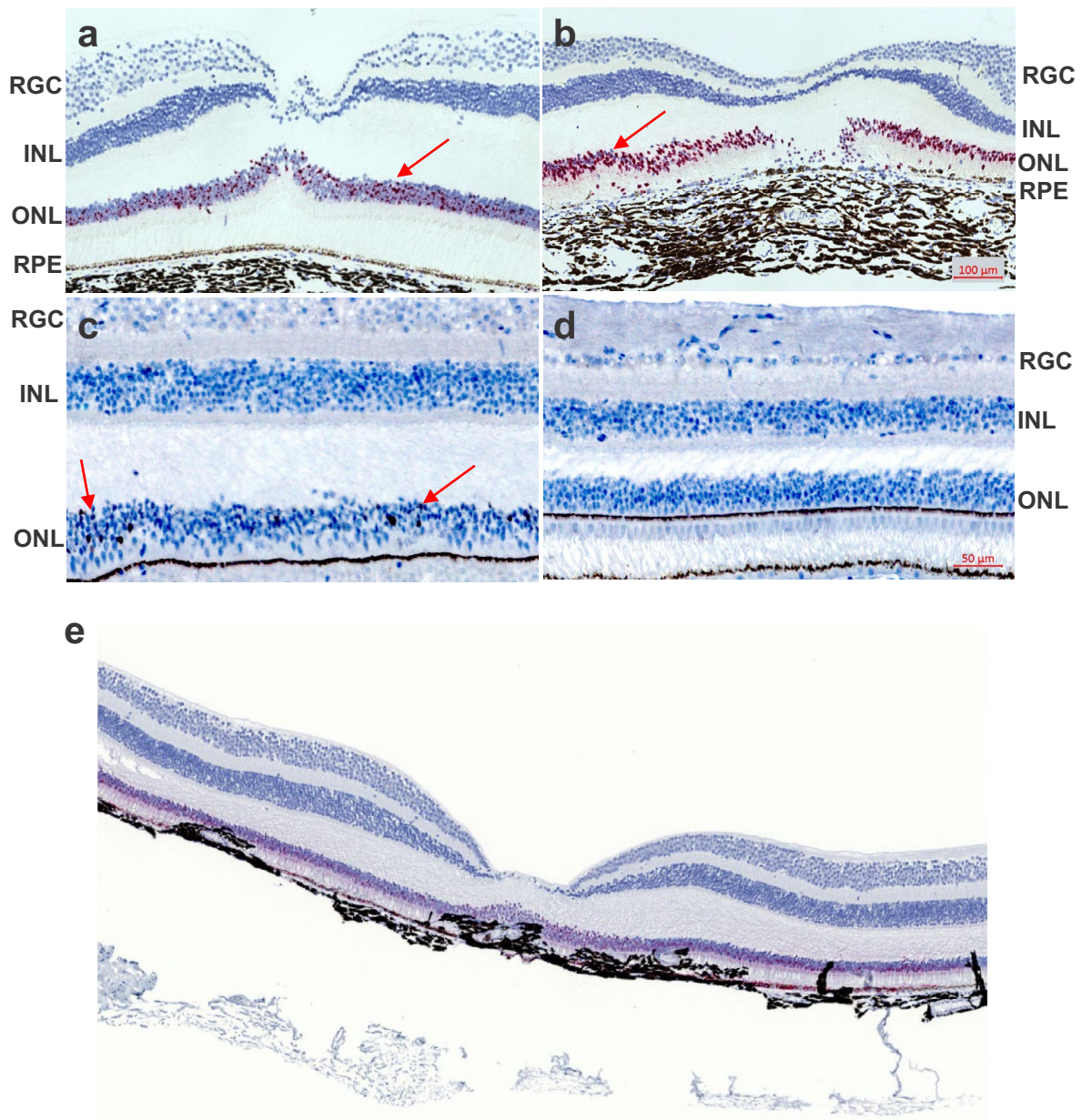
Extended Data Fig. 3 | Specificity profiling of CEP290 gRNAs 323 and 64. a, Digenome-Seq was used to identify cuts across the genome. The positive control, SpCas9-EMX1, showed dose responsiveness with an increased number of cut sites as RNP concentration increased. No cut sites, other than the on-target site, were identified for guide 64 and only one cut site was detected at the highest concentration (1,000 nM) for guide 323. That candidate off-target site was located in intron 2 of gene CTD-2058B24.2, an 'anti-sense RNA' with no ascribed function; the cut site is close to, but distinct from, an annotated DNase-hypersensitive region. The raw data associated with this figure are available in Supplementary Tables 6 and 7. **b,** Targeted amplicon sequencing of candidate off-target sites in cell lines nucleofected with plasmids and human retinal explants transduced with EDIT-101. Off-target sites are plotted on the x axis and grouped into categories (on-target sites, detection below the lowest level of detection, and detection above the lowest level of detection with no change relative to control), then sorted by mean indel percentage. The y axis is a log scale plot of indels detected at the predicted cut site ± 2 bases. The raw data associated with this figure are available in Supplementary Table 8. **c,** Summary table of candidate off-target site-targeted sequencing. See detailed list in Supplementary Table 8.



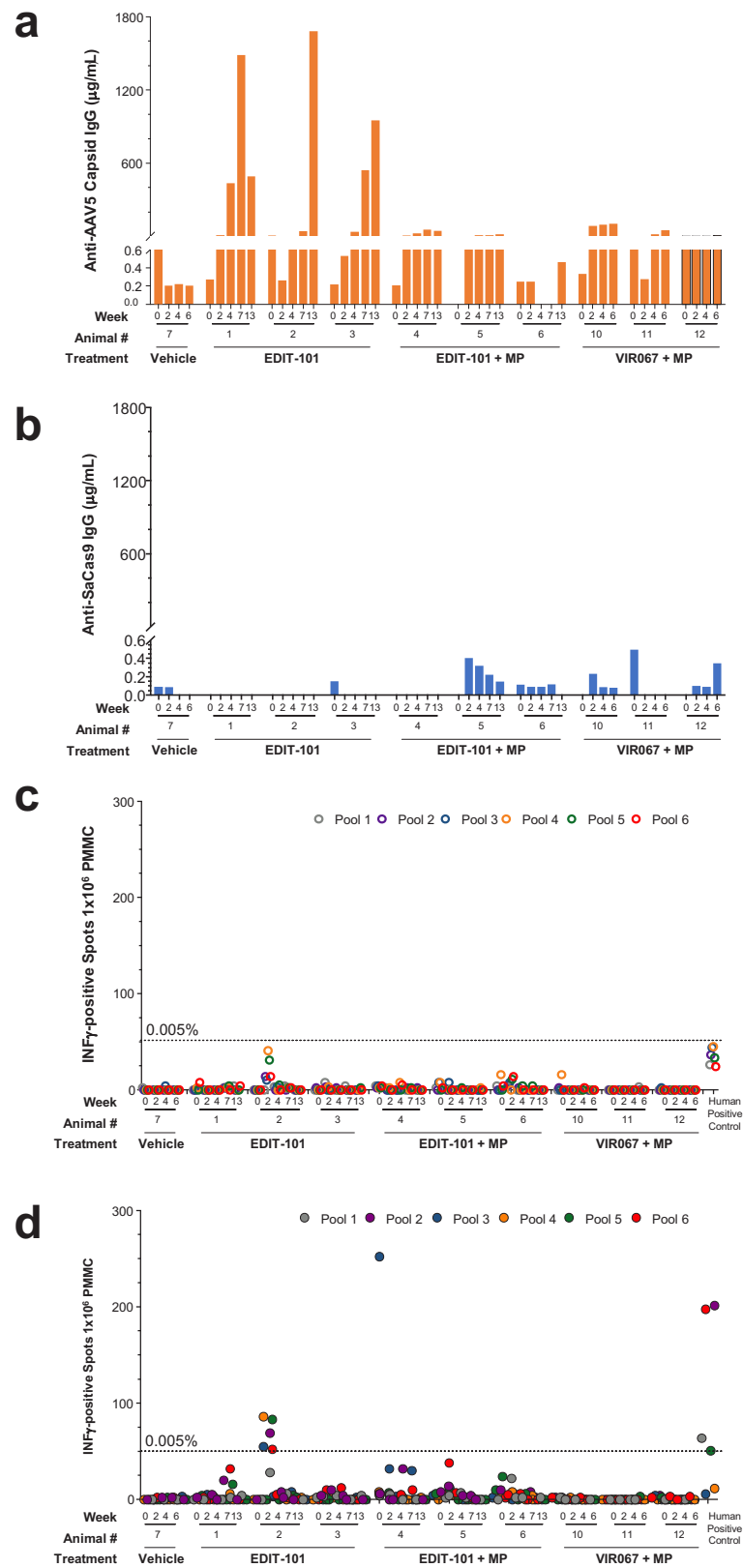
Extended Data Fig. 4 | Transduction and editing efficiency of mouse neural retina by subretinal injection of 1 μ l of AAV5 vectors. **a, A representative image of a flat-mounted retina from an HuCEP290 IVS26 KI mouse administered AAV5-GKR1-GFP. The red line outlines the retina, and the GFP-positive area is colored white. **b**, Total editing rates, as quantified by UDiTaS, in genomic DNA isolated from either total retinal cells or fluorescent-activated cell sorter-isolated GFP-positive retinal cells following subretinal injection of EDIT-101 and AAV5-GRK1-GFP in mice. Each bar represents one mouse eye.**



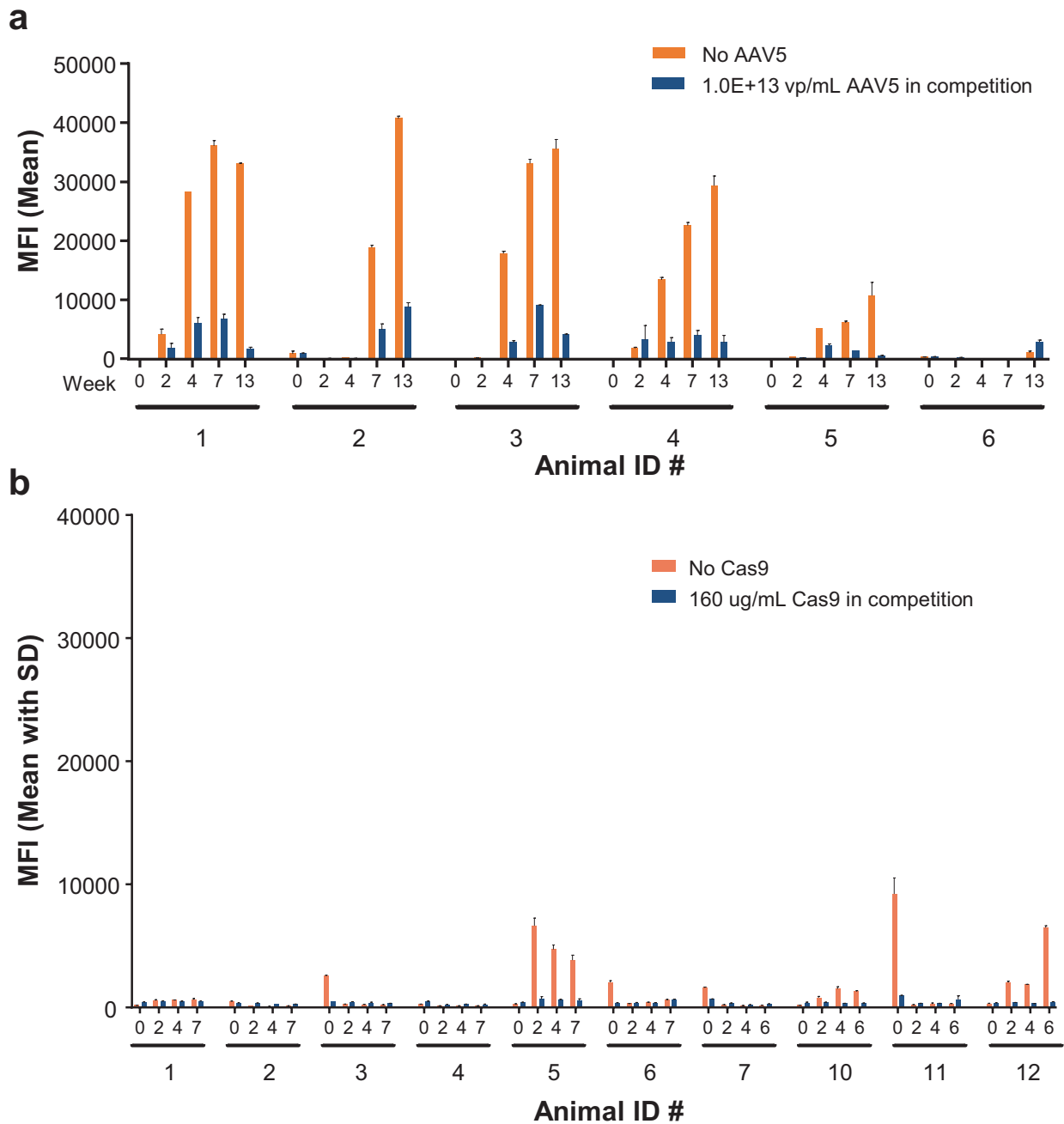
Extended Data Fig. 5 | Comparison of human CEP290 gRNAs and NHP surrogate guides. HuCEP290 IVS26 KI mice were subretinally injected with 1 μ l of either EDIT-101 (blue) or NHP surrogate vector (VIR067, orange) at varying doses. Total editing was quantified by UDiTaS. Each point represents a single mouse eye and error bars represent mean and standard deviation. There was no significant difference found between EDIT-101 and VIR067 at any dose.



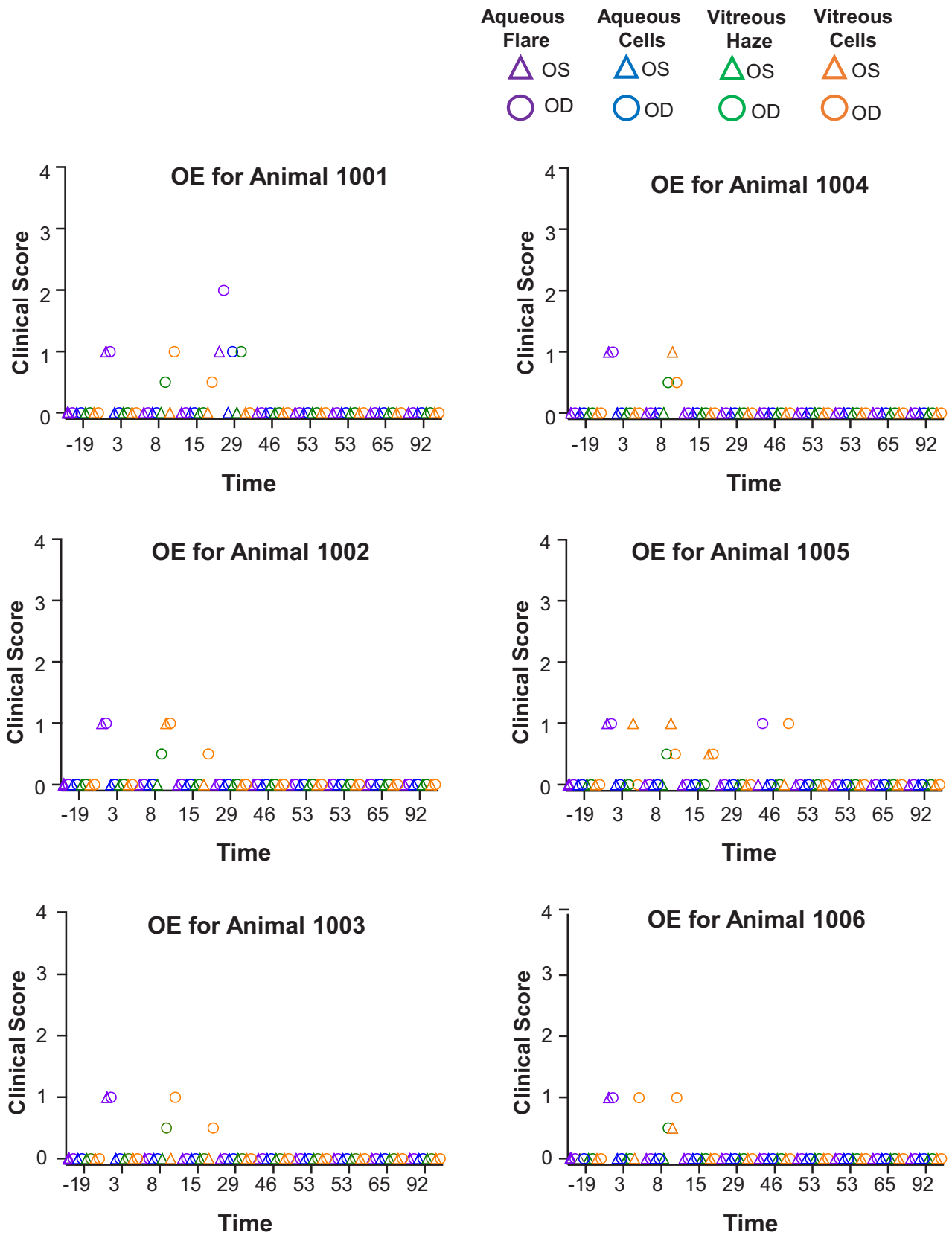
Extended Data Fig. 6 | Localization of AAV genomes and SaCas9 protein in NHPs subretinally injected with VIRO26. **a, b**, Detection of AAV5 vector genome in photoreceptor cells of NHP retina from animals treated with either 1×10^{11} vg ml⁻¹ (**a**, animal no. I16464) or 1×10^{12} vg ml⁻¹ (**b**, animal no. I16467) and assayed at 13 weeks post-dosing. In situ hybridization with a probe specific for the vector genome shows positive staining enriched in the outer nuclear layer (red, arrow). The area of positive staining was quantified on $\times 20$ stitched tiles. Scale bar, 100 μ m. The experiment was performed on six retinas from six different animals treated with VIRO26. **c, d**, Anti-Cas9 immunohistochemistry in monkey no. I6467 showing positive staining in the photoreceptor nuclear layer (arrows) within the bleb region (**c**) but not outside of the bleb on the opposite side of the optic nerve (**d**). $\times 20$ stitched tiles. Scale bar, 50 μ m. The experiment was performed on six retinas from six different animals treated with VIRO26. **e**, Detection of AAV5 vector genome in photoreceptor cells of NHP 1012 OD showing positive staining encompassing the foveal area (red). $\times 20$ stitched tiles. OD: right eye.



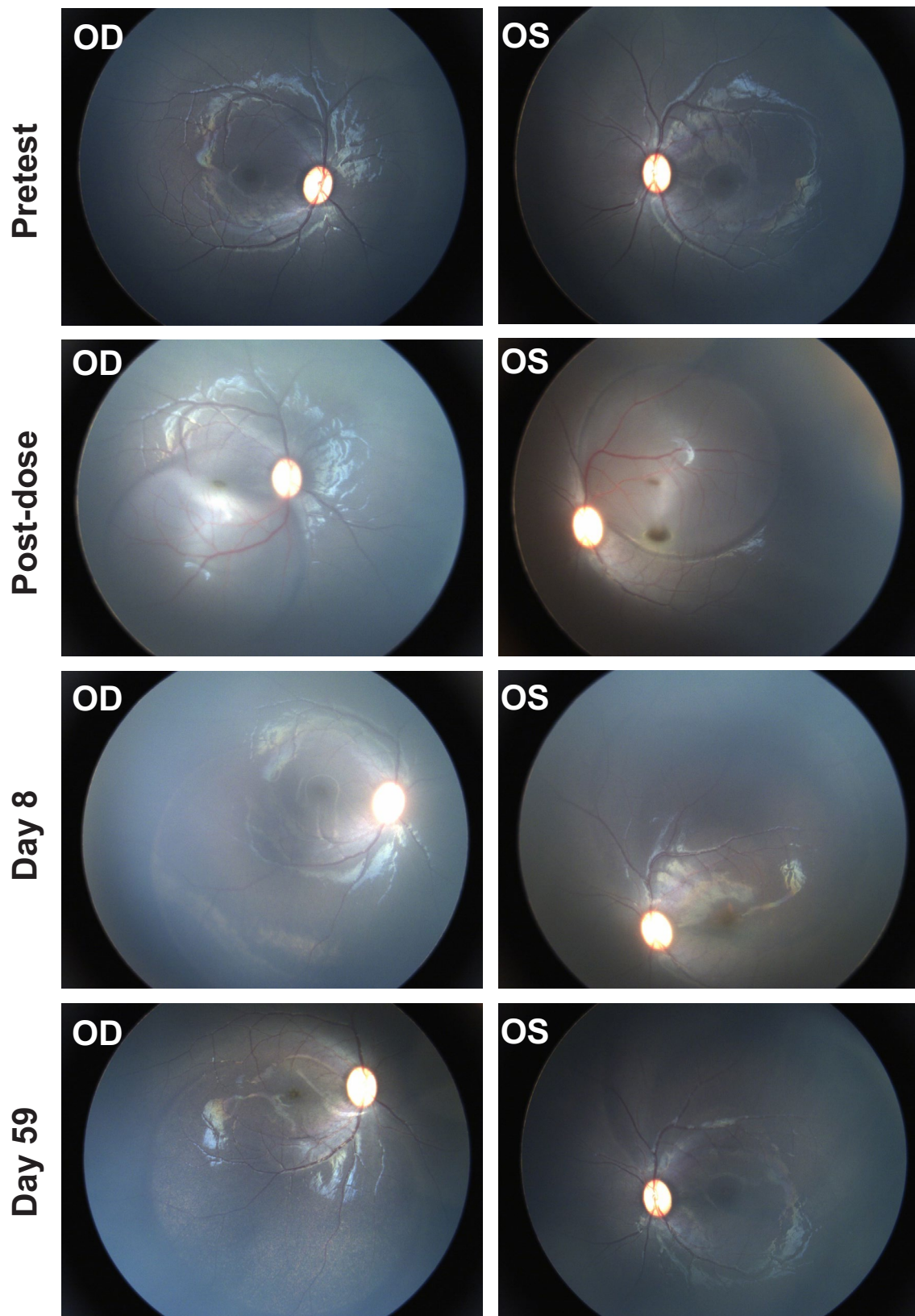
Extended Data Fig. 7 | Immunogenicity assessment of AAV5-CRISPR/Cas9-based in vivo genome editing in NHPs. a,b, Antibodies against AAV5 capsid protein (**a**) and Cas9 protein (**b**) were measured in sera from the study animals using a Luminex bead-based assay. Results are presented as concentration of IgG against AAV5 and Cas9 in each individual animal's serum at each time point. All samples were run in triplicate. **c,d,** ELISpots were performed to measure Cas9-specific CD8 T-cell responses (**c**) and Cas9-specific CD4 T-cell responses (**d**). Peripheral blood mononuclear cells from individual animals were stimulated with Cas9 peptide pools and assayed for IFN- γ production. Data are presented as the number of IFN- γ spot-forming cells per million cells.



Extended Data Fig. 8 | Inhibition of anti-Cas9 and anti-AAV5 antibody binding with excess antigen. a,b, To confirm antibody specificity, animal serum was pre-incubated with excess AAV5 capsid protein, 1×10^{13} viral particles ml^{-1} (**a**) or excess Cas9 protein, $160 \mu\text{g} \text{ml}^{-1}$ (**b**). Reduction in antibody binding, denoted by a decrease in median fluorescence intensity, was measured using the Luminex bead platform.



Extended Data Fig. 9 | Ocular tolerability. Scoring of anterior and posterior changes based on modifications of the Standardization of Uveitis Nomenclature, Hackett-McDonald and Semi-quantitative Preclinical Ocular Toxicology Scoring systems.



Extended Data Fig. 10 | Representative fundus image. Representative fundus images from animal no. 1005 (treated OD with EDIT-101 at 1×10^{12} vg ml⁻¹ and OS with vehicle) at pre-test, post-dosing and days 8 and 59, showing submacular bleb formation. Fundus imaging was performed with similar results for all 16 NHPs reported in this study, and is detailed in Supplementary Table 9. OD: right eye; OS: left eye.

Reporting Summary

Nature Research wishes to improve the reproducibility of the work that we publish. This form provides structure for consistency and transparency in reporting. For further information on Nature Research policies, see [Authors & Referees](#) and the [Editorial Policy Checklist](#).

Statistical parameters

When statistical analyses are reported, confirm that the following items are present in the relevant location (e.g. figure legend, table legend, main text, or Methods section).

n/a Confirmed

- The exact sample size (n) for each experimental group/condition, given as a discrete number and unit of measurement
- An indication of whether measurements were taken from distinct samples or whether the same sample was measured repeatedly
- The statistical test(s) used AND whether they are one- or two-sided
Only common tests should be described solely by name; describe more complex techniques in the Methods section.
- A description of all covariates tested
- A description of any assumptions or corrections, such as tests of normality and adjustment for multiple comparisons
- A full description of the statistics including central tendency (e.g. means) or other basic estimates (e.g. regression coefficient) AND variation (e.g. standard deviation) or associated estimates of uncertainty (e.g. confidence intervals)
- For null hypothesis testing, the test statistic (e.g. F , t , r) with confidence intervals, effect sizes, degrees of freedom and P value noted
Give P values as exact values whenever suitable.
- For Bayesian analysis, information on the choice of priors and Markov chain Monte Carlo settings
- For hierarchical and complex designs, identification of the appropriate level for tests and full reporting of outcomes
- Estimates of effect sizes (e.g. Cohen's d , Pearson's r), indicating how they were calculated
- Clearly defined error bars
State explicitly what error bars represent (e.g. SD , SE , CI)

Our web collection on [statistics for biologists](#) may be useful.

Software and code

Policy information about [availability of computer code](#)

Data collection

Data collection was performed by instrumentation software (ex. Illumina miseq pre-installed software, ImmunoSpot software). Software specific to instrumentation is described in the methods.

Data analysis

Microsoft Excel, Prism (7.0d) and Tableau was used for statistical analysis and data visualization. UDiTaS analysis was described in Gianakos et al 2018 and the code is available on GitHub at (<https://github.com/editasmedicine>). Targeted PCR-NGS analysis was described in Bothmer et al 2017 with exceptions noted in the methods. Sequencing data was aligned to GRCh38 using bwa mem version 0.7.17 and duplicate marked using Picard 2.17.0. GUIDE-Seq analysis was described in Tsai et al 2015 and Friedland et al 2015. Digenome-Seq analysis used custom code that was conceptually similar to work described in Park et al 2017. We plan to make the Digenome code available on github with publication of this manuscript. Cas-OFFinder was described in Bae et al 2014.

For manuscripts utilizing custom algorithms or software that are central to the research but not yet described in published literature, software must be made available to editors/reviewers upon request. We strongly encourage code deposition in a community repository (e.g. GitHub). See the Nature Research [guidelines for submitting code & software](#) for further information.

Data

Policy information about [availability of data](#)

All manuscripts must include a [data availability statement](#). This statement should provide the following information, where applicable:

- Accession codes, unique identifiers, or web links for publicly available datasets
- A list of figures that have associated raw data
- A description of any restrictions on data availability

Detailed data analysis is available in the Extended Data tables of this manuscript. All requests for raw data are promptly reviewed by the CSO or CTO of Editas Medicine and any data that can be shared will be released to requestor. WGS data are available via the NCBI-SRA database PRJNA497602.

Field-specific reporting

Please select the best fit for your research. If you are not sure, read the appropriate sections before making your selection.

Life sciences Behavioural & social sciences Ecological, evolutionary & environmental sciences

For a reference copy of the document with all sections, see nature.com/authors/policies/ReportingSummary-flat.pdf

Life sciences study design

All studies must disclose on these points even when the disclosure is negative.

Sample size	No sample size calculation was used to predetermine sample sizes. Sample sizes for monkeys were limited by cost and the desire to conserve primate usage. Sample sizes for mice were typically 5 mice (10 eyes) per cohort, as this is a standard size cohort for mouse studies. These sample sizes were sufficient to achieve statistical significance.
Data exclusions	Mice with poor or failed subretinal injections (as determined visually at the time of injection) were excluded. NGS runs for targeted amplicon sequencing with fewer than 10,000 sequencing. Both of these exclusion criteria we pre-established prior to initiation of experiment.
Replication	Almost all experiments were performed with separate biological replicates and the data successfully replicated. Monkey experiments were not replicated due to the cost and the desire to conserve number of primates used.
Randomization	Animals were randomly assigned to groups.
Blinding	Yes, the people running the experimental analysis (ex. sequencing, RT-qPCR) did not know which group each sample came from at the time of the experiment.

Reporting for specific materials, systems and methods

Materials & experimental systems

n/a	Involved in the study
<input checked="" type="checkbox"/>	<input type="checkbox"/> Unique biological materials
<input type="checkbox"/>	<input checked="" type="checkbox"/> Antibodies
<input type="checkbox"/>	<input checked="" type="checkbox"/> Eukaryotic cell lines
<input checked="" type="checkbox"/>	<input type="checkbox"/> Palaeontology
<input type="checkbox"/>	<input checked="" type="checkbox"/> Animals and other organisms
<input type="checkbox"/>	<input checked="" type="checkbox"/> Human research participants

Methods

n/a	Involved in the study
<input checked="" type="checkbox"/>	<input type="checkbox"/> ChIP-seq
<input checked="" type="checkbox"/>	<input type="checkbox"/> Flow cytometry
<input checked="" type="checkbox"/>	<input type="checkbox"/> MRI-based neuroimaging

Antibodies

Antibodies used

For WB: CEP290 primary antibody (Abcam #ab128231) at 1:250 dilution, rabbit monoclonal anti-Cas9 antibody (Abcam, ab203943). For IHC: Rabbit anti-Cas9 antibodies (Abcam #ab203933 lot GR3303474-5 and #ab203943 lot GR3191511-3) at final concentrations of 0.1, 1 and 10ug/ml and chick polyclonal anti-GFP antibody (Abcam #ab13970 lot GR236651-17) at a concentration of 1ul/ml. For ELISpot: Human/NHP IFN-gamma/IL2 Capture (Cellular Technology Limited Cat #hT2002F) diluted 1:250, Human/NHP IFN-gamma detection (Cellular Technology Limited #hT02) diluted 1:250, Human/NHP IL2 detection (Cellular Technology Limited #hT16) diluted 1:100. For ADA: ADK5a – (Anti-AAV5) OriGene Tecnologies Cat BM5095 used in the standard curve from 20,000 ng/mL to 0.128 ng/mL, Biotinylated ProG (Thermo Fisher CAT 29988) is used as a cross-species IgG detection

and is used at 2 ug/mL and 100 uL is used, Streptavidin PE (Luminex CAT GR035C0367) is used as the reporter and is used at 4 ug/mL (again 100 uL is used).

Validation

For anti-CEP290 antibody: Drivas TG et al. Disruption of CEP290 microtubule/membrane-binding domains causes retinal degeneration. J Clin Invest 123:4525-39 (2013).
For anti-Cas9 antibody: Abcam website shows validation by confocal imaging, flow cytometry, immunoprecipitation and Western blots of HEK293 cells transfected with Cas9 expression plasmid, and untransfected controls.

Our own experiments with both include negative controls to demonstrate specificity.

Eukaryotic cell lines

Policy information about [cell lines](#)

Cell line source(s)

Primary patient fibroblasts from the University of Iowa, U2OS cells from ATCC, ARPE19 cells from ATCC, SH-SY5Y cells from ATCC, HEK293 and HEK293T cells from ATCC

Authentication

authentication only by observation of correct morphology

Mycoplasma contamination

All cell lines tested negative for mycoplasma

Commonly misidentified lines (See [ICLAC](#) register)

none

Animals and other organisms

Policy information about [studies involving animals](#); [ARRIVE guidelines](#) recommended for reporting animal research

Laboratory animals

Mice: Mixed C57Bl/6, DBA2 & 129 OLA background, 6-12 wks-old, mix-gender; NHPs: Macaca fascicularis, mixed-gender, 2-4years old

Wild animals

The study did not involve any wild animals

Field-collected samples

The study did not involve and field-collected samples

Human research participants

Policy information about [studies involving human research participants](#)

Population characteristics

N/A

Recruitment

Patients were recruited by the University of Iowa based on the diagnosis of CEP290-associated retinal degeneration with at least one IVS26 c.2991+1655A>G mutation.